Liquid Crystalline Gelation of DNA

A doctoral thesis submitted to Gunma University

March 2008

Kazuya Furusawa

05802206

Faculty of Engineering, Gunma University,

Kiryu, Gunma, Japan

Contents

Overview 3

Chapter 1 Liquid Crystalline Gelation of DNA aqueous solution
- 1.1 Introduction 6
- 1.2 Experimental Section 7
- 1.3 Results and Discussion 9

Chapter 2 Dynamics of Liquid Crystalline Gelation of DNA
- 2.1 Introduction 19
- 2.2 Experiments 20
- 2.3 Theoretical Background 23
- 2.4 Results 25
- 2.5 Disucussion 27

Chapter 3 Adsorption Kinetics of Carcinogens to DNA Liquid Crystalline Gel Beads
- 3.1 Introduction 46
- 3.2 Experiments 47
- 3.3 Theoretical Analysis 48
- 3.4 Results 54
- 3.5 Disucussion 55

Summary 68

References 70

Acknowledgments 73

List of publications 74

Introduction

Deoxyribonucleic acid (DNA) is a linear polymer having a double helix structure and negative charges along the chain (1-4). The DNA molecules have various biochemical functions in animate beings. The main role of DNA is the carrier of genetic information from one generation to the next (5-6). In recent years, many efforts have been devoted to develop materials consisting of DNA as a functional polymer (7-13). As a typical example, carcinogenic agents and environmental hormones having planar aromatic groups intercalate into DNA double helices (4,14-15), resulting in inhibition of interpretation of hereditary code (16). This specific property of DNA is used as the most efficient adsorbents of such specific toxic agents selectively. For this application, DNA must be in a water-insoluble state. Several technological developments to prepare water-insoluble DNA compounds have been performed to create environmental cleanup materials (7-11). Nishi et al. succeeded in the insolubilization of salmon milt DNA by cross-linking it with ultraviolet irradiation (8-10) and by forming molecular complexes with other biomacromolecules (7). Umeno et al. reported the synthesis and characterization of polyacrylamide gels containing DNA and their application as carcinogen absorbents (11).

At the concentrated states, DNA forms various lyotropic liquid crystalline phases depending on the DNA concentration and the ion strength (17-21). On the other hands, isotropic gels consisting of DNA prepared by using chemical cross-linking reagents and metal cations have been reported (22-23). Recently, we have found that a dialysis of concentrated solutions of rigid or semi-flexible polymer molecules such as curdlan and DNA in concentrated aqueous metal multivalent cations (such as Ca^{2+}, Mg^{2+}, Co^{2+}, Ni^{2+},

Mn^{2+}, Fe^{2+}, Cu^{2+}, Dy^{2+} and Al^{3+}) yields cylindrical liquid crystalline gel (LCG) in the dialysis tube (24-25). This new material is expected to be utilized as an intelligent probe and an adsorbent of toxic agents with advantage of anisotropic optical properties and high capacity of holding solvents. In this doctor's thesis, a mechanism of liquid crystalline gelation of DNA aqueous solution is studied from experimental and theoretical aspects, and adsorption kinetics of carcinogenic agents to DNA LCG is also investigated.

In Chapter 2, the preparation method and the condition for forming DNA LCG were described. Various forms of DNA LCG, such as a bead, a film, and a fiber, were successfully prepared by using an insolubilization reaction method. The gel and optical properties of DNA LCG were also discussed. The adsorption capacity of carcinogenic agents of DNA LCG beads was investigated.

In Chapter 3, the process of forming DNA LCG is investigated experimentally and theoretically. Since the ordered structure in the LCG formed in the process has considerable effects on the characteristic properies of DNA LCG, such as birefringence and Young's modulus, it is important to understand the dynamics of liquid crystalline gelation. To trace the process, DNA LCG films was prepared by immersing DNA aqueous borate solutions sandwiched between two circular glass plates into cobalt chloride solutions. To explain the dynamics of DNA liquid crystalline gelation, a theory based on the nonequilibrium thermodynamics with "moving boundary picture" (26) was modified, and the results were analyzed by the modified theory.

In Chapter 4, the adsorption kinetics of carcinogenic agents to DNA LCG beads is described. The kinetics of adsorption of toxic agents by DNA molecules has been studied (27-28), and the interaction was classified into external binding, groove binding

and intercalation. Especially, ethidium-DNA intercalation has been intensively investigated (29-30), and multistep kinetics has been proposed. Although the mechanism of adsorption of toxic agents into DNA composites could be explained by the combination of the above essential interactions, from the aspect of bioconjugate materials science and technology, it is more important to describe the adsorption behavior phenomenologically, because meso- and macro-scale structures of the composites have considerable effects on the adsorption behavior. To understand the adsorption behavior, a theory for the adsorption kinetics of carcinogens to DNA LCG beads has been developed by using the non-equilibrium thermodynamics with simple assumptions.

Chapter 1

Liquid Crystalline Gelation of DNA Aqueous Solution

1.1 Introduction

LCG is of current interest for its large capacity of adsorbing solvent and LCG's unique optical characteristics. Gelation and liquid-crystal formation are, however, usually conflicting with each other since gels are isotropic materials swollen with a large amount of solvent and liquid crystals are anisotropic materials composed of rodlike molecules aligning at least in one direction. Therefore, LCGs have been prepared by somewhat ad hoc maneuvers, such as embedding rodlike molecules in reactive multifunctional monomers, which can cross-link each other (31). It is also well-known that DNA LCG has been prepared by forming a DNA-surfactant complex, where surfactant-nucleotide interaction makes cross-linking points (12). Recently, M. Nobe et al. reported a new method to prepare LCG by self-organization of one of rod-like polysaccharides, triple helical curdlan in aqueous NaOH in a process of dialysis to aqueous $CaCl_2$ (24,26, 32-33). Slow dynamics of concentrated Curdlan solution resulting from an outflow of hydroxide anions and sodium cations are combined by an inflow of calcium cations and chloride anions through dialysis membrane. Random coil to triple helix transformation of Curdlan molecules by lowering pH and cross-linking of Curdlan molecules by calcium cations were coupled to form LCG in the process. It is hoped that this methodology for preparing LCG could be applied to other combinations of rodlike polymers and aqueous metal salts.

Double helical DNA is a typical rodlike biopolymer having persistence length of 500 Å and minus charges at each 1.5Å along the rod in dilute solutions (4), and forms a lyotropic liquid crystalline phase in concentrated solutions (17-21). On the other hand, "isotropic" chemical gelation of DNA with cross-linking reagents or metal cations has been reported (22-23). Therefore, it seems to be appropriate to apply the above method for preparing LCG to DNA.

In this chapter, the condition for finding DNA LCG is examined by means of the insolubilization reaction used for microencapsulation (34) and the mechanism for forming DNA LCG is discussed. The adsorption of one of carcinogenic agents, acridine orange, to the DNA LCG is demonstrated.

1.2 Experimental Section

An appropriate amount of sodium-type double-helical DNA with 10kbp from salmon milt (Nippon Chemical Feed Co. Ltd.) was dissolved in a buffer solution (40 mM sodium borate and 10 mM sodium chloride at pH 9.2) at 1 or 3 % of weight (15 mM nucleotide). The solution was dialyzed into 100 mM cobalt chloride by the following two methods and used for different parts of the experiment. (1) To characterize the degree of orientation of DNA molecules, 5 mL of the DNA solution was poured into a dialysis tube with d_0 = 6mm-25mm diameter (Sanko Pure Chemical Co. Ltd.) and dialyzed into 200 mL of aqueous cobalt chloride of various concentrations for 24h to form an LCG cylinder. Cross-sectional strips were excised in directions perpendicular to and parallel with the long axis of the dialysis tubes to be observed under natural light and crossed nicols. After the dialysis the cross-sectional diameter d_f and the thickness of the LCG layer δ_{LCG} was measured. The shrinking ratio s defined as $s = (d_0-d_f)/d_0$ was

obtained. (2) To find the condition of preparing LCG, 1wt% DNA solution in a syringe with different gauges was dripped into aqueous cobalt chloride to prepare LCG microspheres. When a droplet of the viscous concentrated DNA solutions buffered by boric acid is dipped into the reactive fluid of aqueous cobalt chloride, insolubilization reaction occurs on the spherical surface of the droplet. The interfacial layer formed by the initial reaction played the role of the dialysis tubing, and the dialysis from the spherical surface was realized to make small beads with the diameter of 2-3 mm. Gel was identified by the conventional extrusion method and liquid crystal was identified using crossed nicols. The weight percentage of DNA, W_{DNA}, and molar concentration of cobalt chloride, C_{Co}, were varied in the experiment. The latter experiment was also tried for extradialytic aqueous solutions of different salts of LiCl, NaCl, KCl, $CaCl_2$, $MgCl_2$, $BaCl_2$, $SrCl_2$, $MnCl_2$, $CoCl_2$, $NiCl_2$, $FeCl_2$, $Dy(CH_3COO)_2$ and $AlCl_3$ at a salt concentration of 100 mM. All the salts were purchased from Wako Pure Chemicals and used without further purifications, and MilliQ water was used to dissolve the salts. To examine the effect of buffer for dissolving DNA, 0.5 M 2-amino-2-hydroxymethyl-1,3-propanediol (Tris)-HCl buffer at pH 9.2, 0.1 M phosphate buffer at pH 7.0, 20 vol% ethanol aqueous solution and pure water were used in place of sodium borate as an alternative buffer. The dialysis time was 5min. All the preparations and measurements were made at room temperature of 24 ^{o}C. To assess the capacity of adsorbing acridine orange, 0.05 g of DNALCG beads were immersed into 1.8 mL of acridine orange solutions with concentration in the range between 5 and 1000 μg/mL for 48 h. The optical density at wavelength λ = 495 nm was measured for the solutions before and after immersing the beads. The grams of acridine orange adsorbed to 1 g of DNA LCG microcapsules w_{AO} was caluculated as a function of

weight concentration of acridine orange in dispersing solution c_i from the optical density using a calibration curve.

1.3 Results and Discussion

In the course of the dialysis process the DNA solution gelled and a birefringence increasingly appeared. Figure 1 shows the upper view of the cross-sectional strip perpendicular to the long axis of the DNA (3 wt%) gel with the thickness of 6 mm observed under crossed nicols. Black cross lines were also observed as shown in Figure 1. The corresponding colored layer and black cross line were also observed in the side view of the strip excised parallel to the long axis along the center line, whereas no transmitted light was observed for the strips excised parallel to the long axis along off-center lines under the crossed nicols (not shown). These results indicate the radial ordering of DNA molecules or their aggregates, i.e., the LCG formation. The DNA solution in the inner core of the gel observed black (no transmitted light) was more dilute than that in the original solution and easily washed out to form a hollow cylinder when the dialysis time t_D was less than 3h for the diameter of the dialysis membrane being 16mm. At t_D>3h, the whole cylinder gelled, but the core of the cylinder was very soft and fragile. The diameter decreased in the course of dialysis by about 16% and; i.e., the inner volume of the dialysis tube became about 60% of the initial volume. The shrinking ratio was independent of the diameter of the dialysis tube, as shown in Fig. 2. The thickness of the LCG layer after the dialysis for t_D>3h was proportional to the diameter of the dialysis tube, as shown in Fig. 3, and to the diameter of the gel after the dialysis.

This proportional relation is explained as follows. The DNA solution becames

concentrated to form the liquid-crystalline structures. Therefore, the DNA concentration in the LCG layer ρ_{LCG} is larger than that in the original solution ρ_0. The DNA concentration in the sol phase ρ_s decreases as the LCG layer grows. When ρ_s reaches a minimum concentration $\rho_{\min}$, the LCG layer growth would stop. The conservation law of the DNA molecule number leads to a simple relation

$$\pi(\frac{d_0}{2})^2\rho_0 = \pi[(\frac{d_0}{2})^2 - (\frac{d_0}{2} - \delta_{DNA})^2]\rho_{LCG} + \pi(\frac{d_0}{2} - \delta_{DNA})^2\rho_{\min} \quad (1)$$

From the above, we have the relationship between the thickness of the outer liquid crystal layer δ_{DNA} and the diameter of the dialysis tube d_0.

$$\delta_{DNA} = C'd_0 \quad (2)$$

with

$$C' = \frac{1}{2}\left[1 - \sqrt{1 - \frac{\rho_0 - \rho_{\min}}{\rho_{LCG} - \rho_{\min}}}\right] \quad (3)$$

The shrinking effect of the LCG may modify the expression Eq.3 of the coefficient C', but does not change the proportional relation Eq.2 because the shrinking ratio is independent of d_0 as shown in Figure 2.

LCG phase and isotropic transparent gel phase were observed above threshold concentrations of both DNA and cobalt chloride, at intermediate concentrations and at low concentrations, respectively, as shown in the phase relationship of Figure 4 for boric acid concentration of 20mM. The boundary between LCG and isotropic gel moved to lower DNA and $CoCl_2$ concentrations as boric acid concentration was higher. LCG phase was observed in all the buffers except for dispersing pure water at 1wt% DNA and 100mM $CoCl_2$, and LCG region in the diagram was wider for Tris buffer and

borate buffer. Making LCG with dispersing pure water required DNA concentration of more than 5 wt% at 100mM $CoCl_2$. Therefore, LCG is formed irrespective of buffer if other conditions are optimized, although pH is one of the most important factors in determining the phase relationship. The gel was stable and the birefringence did not change at room temperature in water for 10 month. The gel was also stable at 90^{o}C for 1 h.

In the process of dialysis, the DNA solution turned pink at the contact with the cobalt solution through the dialysis membrane, and next the color of the solution changed to green and then to blue. The color change is attributed to the dehydration of cobalt complex of $[Co(H_2O)_6]^{2+}$ and the production of $[CoCl_4]^{2-}$. DNA LCG was also successfully prepared in extradialytic solutions of $MnCl_2$, $CoCl_2$, $NiCl_2$, $FeCl_2$, $CuCl_2$, $Dy(CH_3COO)_2$ and $AlCl_3$ with all the buffer used and $CaCl_2$, $MgCl_2$, $BaCl_2$, and $SrCl_2$ in 20 vol% ethanol aqueous solution. Much higher DNA concentration around 3-5 wt% was required for forming DNALCG for the latter salts. Alkaline metal chlorides such as LiCl, NaCl and KCl did not induce LCG. Therefore, d-block transition metals such as iron (divalent and trivalent), nickel, and manganese chloride aqueous solution, aluminium (p-block element) chloride and dysprosium (f-block element) acetate easily induced LCG. In contrast, alkaline earth metals (s-block elements) such as calcium, magnesium and barium are marginal in forming LCG. Thus, anisotropy of valence electron orbits of cations might be effective for the association of DNA molecules to make cross-links with ordering. It is also suggested that divalent cations that react with inner base more easily form DNA LCG.

From the experimental results the mechanism for forming DNA LCG is speculated as follows. When concentrated DNA molecules come into contact with an excess amount

of metal cations in extradialytic solutions at the dialysis tube interface, the cations are adsorbed not only into the inner core of the helices to form M-form (the DNA-metal ion complex, in which a divalent metal ion (Zn^{2+}, Ni^{2+}, and Co^{2+}) is incorporated into the center of DNA duplex) but also to the outer surface of the DNA double helices. Here, M-form is not significantly important for forming LCG, since LCG is also formed by aqueous aluminium chloride, which is known not to form M-form, and binding to the inner core of DNA does not contribute to cross-linking. DNA molecules change the conformation from a semi-flexible state to a single globular state by counter-ion condensation in dilute solutions (35-40), whereas in concentrated solutions the intermolecular coupled segment-segment interactions through cations might result in oriented DNA association much faster than the intramolecular conformation change, and the orientation is fixed with the cross-linking via the cations: The transition metal cations are shared among segments of different DNA molecules to make cross-links. The boundary condition at the circular dialysis tube and the cation flow forces the DNA molecules or their aggregates to align radially. The considerable decrease in volume is attributed to this type of ionic condensation. The coupling of conformational change of biomacromolecules and the cross-links due to cations is a scenario similar to the LCG formation of one of polysaccharides, Curdlan, by a simple dialysis into a calcium ion bath, in which single to triple helical conformation change induces LCG (24). The difference of the DNA LCG and curdlan LCG is in the homogeneity and packedness: Curdlan LCG has a birefringence gradient in the radial direction of the layer showing continuous color variation under crossed nicols, and forms a close-packed gel in the range of lower concentrations of Curdlan. This structural difference might be attributed to the much more rapid and larger degree of shrinking of DNA gel, which

results in homogeneous growth of the nucleus of DNA mesogens produced at the dialysis tube surface in the first stage of LCG formation. However, we should not take these differences too seriously, since these could be quantitative ones.

It is interesting to examine the functional abilities of the DNA LCG. As a demonstration, the DNA LCG was immersed in an aqueous solution of one of the cancer-causing agents, acridine orange. Figure 5 shows that grams of acridine orange adsorbed to 1 g of DNA LCG microcapsules w_{AO} as a function of acridine orange concentration in dispersing solution c_i. w_{AO} is proportional to c_i with the slope of 21.5 ml/g up to around 8 x 10^{-4} g/mL and then reaches a constant of 0.018 g/g. This means that acridine orange was in equilibrium between DNA LCG microsphere phase and dispersing solution phase up to c_s ~ 8 x 10^{-4} g/mL, and the maximum adsorption of dried DNA LCG microcapsules is w_{AO}^{sat} ~ 0.018 g/g. From this value the number of acridine orange molecules adsorbed to DNA is estimated as $\frac{C_{AO}^{sat} / M_{AO}}{W_{DNA} / 100 M_{NR}} \approx 1.9$ per one unit pair, where M_{AO} and M_{NR} are the molecular weight of acridine orange and nucleotide pair, respectively, and the weight percentage of DNA W_{DNA} in the gel was estimated from the initial concentration of DNA of 1% and shrinking ratio of 60% as 1.7 wt%. Since acridine orange molecules are trapped in DNA in the major groove of DNA double helix and interstices between base pairs and part of acridine orange would compete with Co^{2+} for binding to DNA LCG, the value obtained seems to be reasonable, and it indicates that acridine orange is effectively adsorbed. This also shows that DNA molecules are not much damaged in the process of LCG formation, and the DNA LCGs newly prepared, are good intercalators as an absorbent of this kind of toxic compounds.

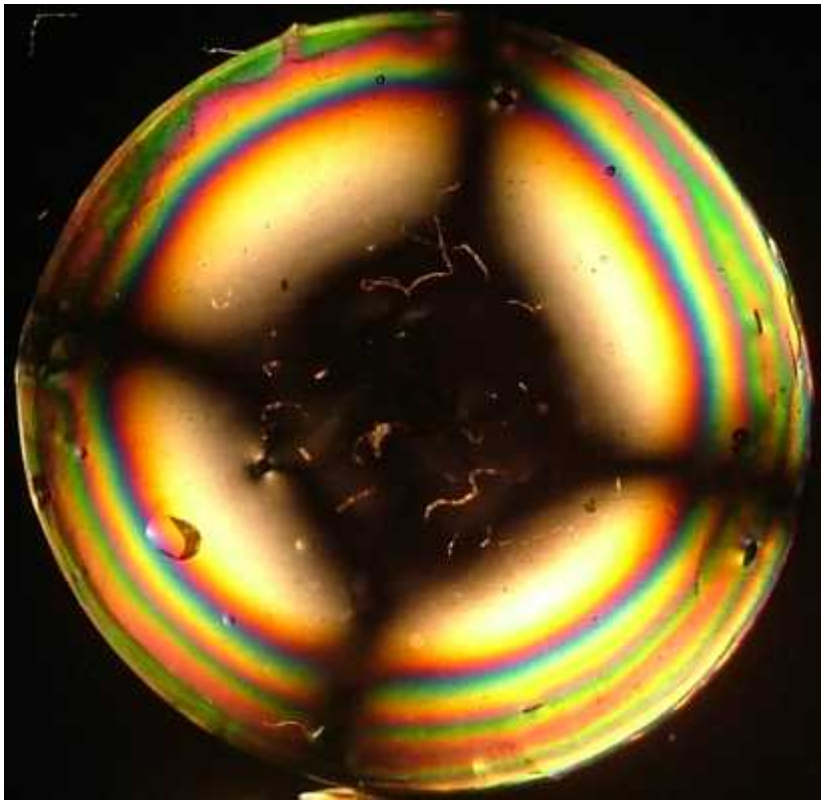

Figure 1. DNA liquid-crystalline gel observed from the upper view of the cross-sectional strip perpendicular to the long axis of dialysis tube under crossed nicols.

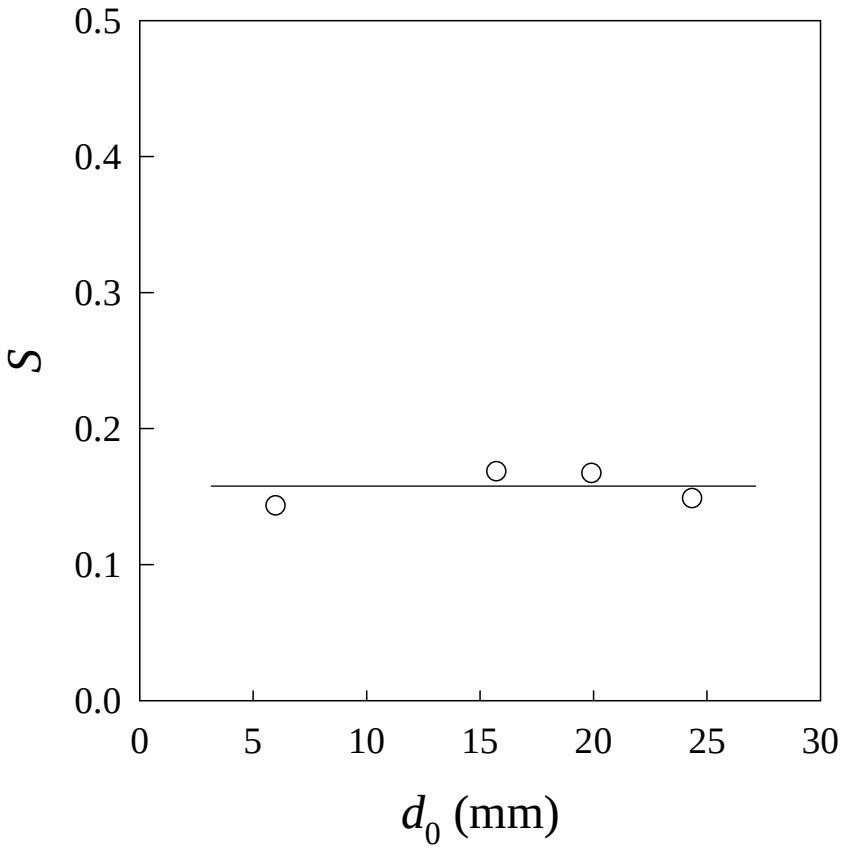

Figure 2. Relationship of the shrinking ratio and the diameter of the dialysis tube.

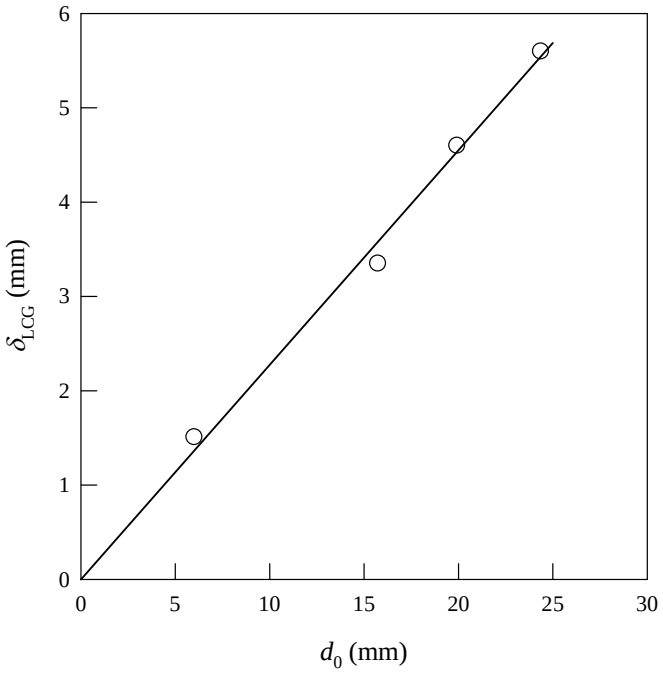

Figure 3. Relationship of the thickness of LCG layer and the diameter of the dialysis tube.

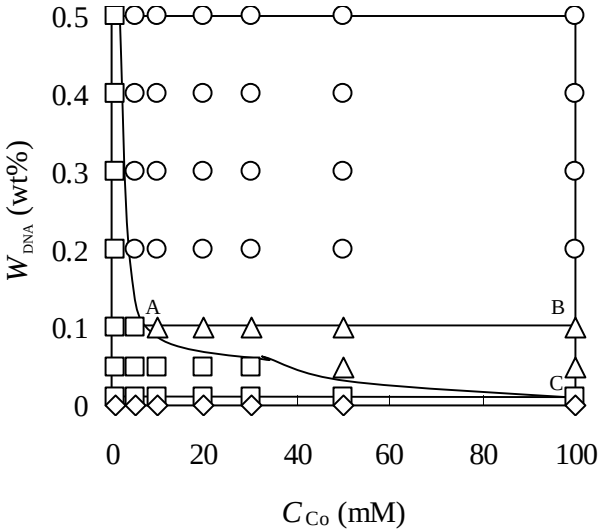

Figure 4. Phase relationship of DNA aqueous cobalt solution at boric acid concentration 20mM. Circles, triangles, squares, and diamonds denote LCG, isotropic gel, coexistence of precipitates and solution, and isotropic solution, respectively. The lines show the roughly estimated phase boundaries. The molar ratios of Co2+ and nuculeotide are ca. 1:2, 1:30, and 1:330 at the points A, B, and C, respectively.

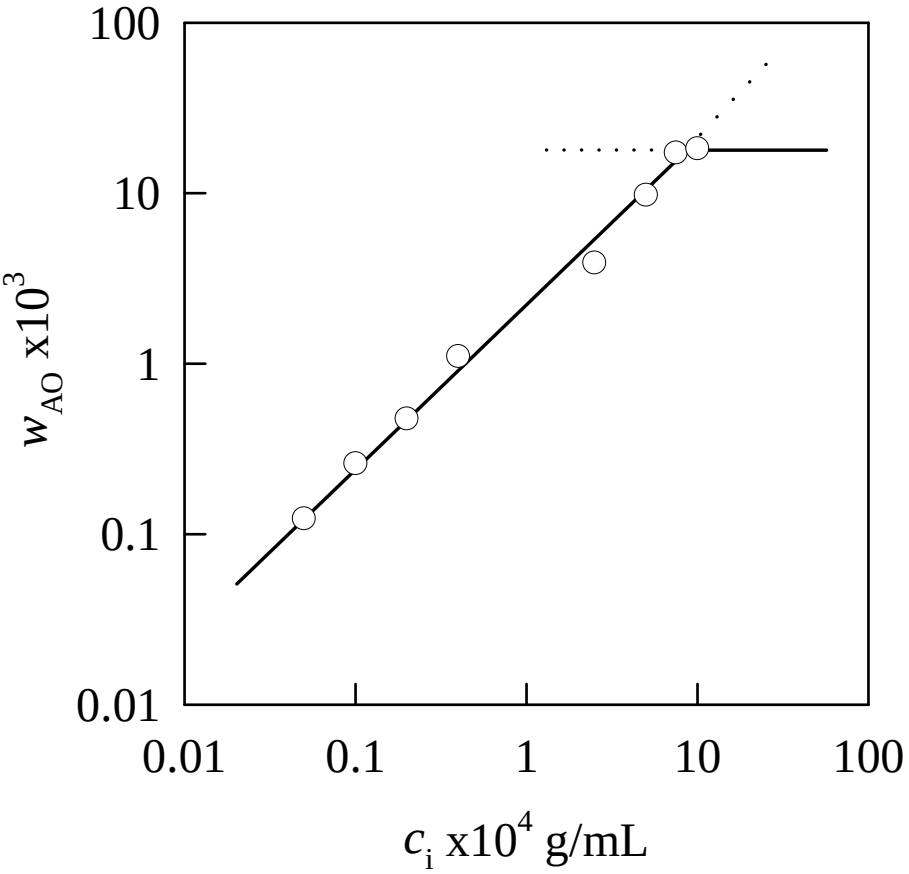

Figure 5. Grams of acridine orange adsorbed to 1 g of DNA LCG microspheres as a function of acridine orange concentration in dispersing solution.

Chapter 2

Dynamics of Liquid Crystalline Gelation of DNA

2.1 Introduction

In chapter 2, we introduced that dialysis of concentrated DNA solutions into concentrated aqueous metal multivalent cations (such as Ca^{2+}, Mg^{2+}, Co^{2+}, Ni^{2+}, Mn^{2+}, Fe^{2+}, Cu^{2+}, Dy^{2+} and Al^{3+}) yields cylindrical liquid crystalline gel (LCG) in the dialysis tube. Formation of the ordered network structure could be attributed to the shear that is induced by cylindrical symmetric flow of metal cations, and is expected to be universal to the systems consisting of intradialytic rigid polymer solutions and extradialytic cross-linking agent solutions separated with a dialysis membrane. During the dialysis, the DNA molecules are both oriented and cross-linked to form LCG from the interface between the extradialytic metal cation solution and the intradialytic DNA solution, i.e., the dialysis membrane. At the final state or after long enough dialysis, however, the DNA gel consists of an outer LCG phase and an inner amorphous gel (AG) phase.

To trace the process quantitatively, in this study, it was attempted that DNA aqueous borate solutions were sandwiched between two circular cover glasses and immersed into concentrated cobalt chloride solutions. Immediately after the immersion, cross-linking reaction occurred at the cylindrical surface between the DNA solution and cobalt chloride solution. Since the interfacial layer formed by the initial reaction played the role of the dialysis membrane, the dialysis from the cylindrical surface was realized.

The time courses of the thickness, the weight fraction of DNA and cobalt cations, the birefringence and the turbidity of the film consisted of outer LCG and inner DNA solution have been measured. The positional dependences of the weight fraction of DNA and cobalt cations were also measured. To explain the DNA LCG formation process, a modification of the theory used for the curdlan LCG formation dynamics (26, 33) was required. The experimental data were explained by the modified theory consistently.

2.2 Experiments

2.2.1 Preparation

Sodium type double stranded DNA extracted and purified from salmon milt was provided by Japan Chemical Feed Co. Ltd. The nominal average base pair examined by the electrophoresis is 10kbp. Cobalt chloride and sodium tetra-borate were purchased from Wako Pure Chemicals. MilliQ water was used as solvent. DNA was dissolved in 20mM sodium tetra-borate aqueous solution at 1.0wt%. This concentration is much lower than the threshold to form DNA liquid crystal without any cationic ions. In order to prepare a DNA LCG film with reference of phase diagram of DNA+ tetra-borate+ cobalt chloride+ water (25), the DNA solution was sandwiched between two circular glass plates with the radius R= 6, 7.5, and 9 mm, and then immersed into 100mM cobalt chloride solution at 20ºC. DNA LCG was formed from the interface between the DNA solution and cobalt chloride solution toward the center of the DNA solution until the critical immersion time t_I for completion of about 120min, 180min, and 240min, respectively for R= 6, 7.5, and 9 mm. The resultant DNA LCG film consisted of an outer LCG layer and an inner amorphous layer at the final state. At the

immersion time $t < t_I$, the inner amorphous layer was solution, whereas at $t > t_I$, the whole solution gelled, but the core of the cylinder was very soft and fragile, where t_I is the time required for gelation of the whole film.

2.2.2 Measurements

(1) Swelling ratio

The thickness $l(t)$ and the cross-sectional area $a(t)$ of DNA aqueous solution (initially) or gel (finally) as shown in Fig. 6 was measured with a cathetometer at immersion time t, and the time course of the shrinking ratios of DNA solution or gel defined as $\gamma(t) = l(t)/l_0$ in thickness and $\gamma(t) = a(t)/a_0$ in cross-sectional area were obtained, where l_0 and a_0 are the thickness and the cross-sectional area of the DNA solution before the immersion, respectively.

(2) DNA and cobalt concentration

The samples prepared at R = 9 mm were sliced concentrically into one to four sections at each immersion time and denoted as S1, S2, S3, and S4 from the outside to the center; S1 (7 mm < r < 9 mm), S2 (5 mm < r < 7 mm), S3 (3 mm < r < 5 mm), and S4 (inner solution region), respectively, where r is the distance from the center. The volume of S4 decreased with t from that of the whole intradialytic solution at the initial state to zero at the final state. The DNA weight fractions of each section w_1 through w_4 corresponding to S1 through S4 were determined at different immersion times (30~480 min) based on the Bartlet method (41): 0.1g of each strip was immersed in 10g of MilliQ water, and 1g of 30% hydrogen peroxide were added to it. 0.6 ml of the solution was mixed with 0.6 ml 10N sulfuric acid in a test tube, and then heated at 180 ^oC for 3 h in an oven. Then the solutions were mixed with 4.4 ml of milliQ water, 0.2 ml

of 5% ammonium molybdate solution, and 0.2 ml of Fisk-Sabbarow reagent solution; 0.125 g of 1-amino-2-naphthol-4-sulfuric acid mixed with 50 ml of 15wt% sodium hydrogen sulfate aqueous solution and 0.25 g of sodium sulfate. They were heated again in boiled water for 7 minutes. The total phosphate concentration was determined by measuring the optical density of the solution at the wavelength of 830 nm. The weight fraction of DNA was calibrated with standard DNA solutions with known weight fractions.

The cobalt concentration C_{Co} was determined by chelatometric back-titration using the sample with R = 9 mm at different immersion times (20~360 min): 0.02g of the outermost LCG layer and inner DNA solution or amorphous gel were used for this measurement. Each sample was dissolved in 20ml of 0.01M Na_2(EDTA·4Na) with gentle stirring of the solution for 24 h and then mixed with 2 ml of ammonium buffer at pH 10. A few drops of eriochrome black T (EBT) were added to the solution as an indicator. The cobalt content of the samples was determined by back-titration using a 0.01M zinc sulfate standard solution.

(3) Birefringence and turbidity

Measurements of birefringence and turbidity of DNA LCG or solution were performed by a laboratory made device (26) for the sample with R = 7.5 mm. The time courses of birefringence and turbidity were measured at a constant position in the outermost portion of the sample, e.g., distance from the center of the circular glass plates r = 7mm. The distance between the liquid crystal front line and the circumference of LCG, i.e., the width of the LCG layer, x was also measured as a function of the immersion time t for the samples with R = 6, 7.5, and 9 mm. This experiment was also done for the samples with 1 wt% DNA and various cobalt chloride

concentrations in the range between 50-800 mM, and with various DNA concentrations in the range between 0.42wt% and 1.2 wt% and 100 mM cobalt chloride, at R = 7.5 mm.

All the measurements were performed at 20°C.

2.3 Theoretical Background

The experimental data of the growth process of DNA LCG formation were analyzed by a theory based on the following assumptions (26). (a) All cobalt cations flowing into the inner polymer solution are used up to produce the LCG layer. (b) The LCG layer does not capture the cobalt cations as a sink; all of the cobalt cations flowing into the LCG layer arrive at the inner polymer solution to realize a steady state. Under the assumptions, only the motion of the boundary between the LCG layer and the sol core is required to express the time course of gelation (the moving boundary picture for the dynamics of LCG formation (26)). Expressing the boundary motion in terms of the LCG layer width $x = x(t)$ and introducing the scaled width $\tilde{x} = x/R$ and the scaled immersion time $\tilde{t} = t/R^2$, we have

$$\tilde{y} \equiv \frac{1}{2}(1-\tilde{x})^2 \ln(1-\tilde{x}) - \frac{1}{4}\tilde{x}^2 + \frac{1}{2}\tilde{x} = K\tilde{t} \qquad (1)$$

where K is related to the diffusion coefficient of cobalt cations $\overline{D}_{Co}$ as

$$\overline{D}_{\mathrm{Co}} \approx \frac{\rho_{\mathrm{g}}}{\rho_{\mathrm{s}}} K \qquad (2)$$

Here, $\overline{D}_{\mathrm{Co}}$, ρ_{g}, and ρ_{s} are the diffusion coefficient of cobalt cations in the LCG layer, the critical concentration of cobalt cations for forming gel, and the concentration of

cobalt cations in extradialytic solution.

Let us review the derivation of eq.(1) briefly. In terms of the concentration of cobalt cations at the distance r from the center in the LCG layer $\rho'(r)$ and the chemical potential of cobalt cations in the LCG layer $\mu_G(\rho')$, the influx velocity of cobalt cations along the radial direction in the LCG layer is expressed as

$$v = k\frac{\partial \mu_G(\rho'(r))}{\partial r} \tag{3}$$

where k is the mobility of cobalt cations. The flux density vector of cobalt cation is given by

$$\begin{aligned} \vec{j}(r) &= -j(r)\vec{\mathrm{e}}_{\mathrm{r}} \\ j(r) &= v\rho'(r) \end{aligned} \tag{4}$$

where $\vec{\mathrm{e}}_{\mathrm{r}}$ is the unit vector along the radial direction. From the assumption (b), we have

$$\mathrm{div}\vec{j} = -\frac{1}{r}\frac{\partial rj}{\partial r} = 0 \tag{5}$$

Using (3) and (5), we have

$$\begin{aligned} j &= \frac{A}{\ln\dfrac{R}{R-x}}\frac{1}{r} \\ A &= k[\rho'_s\mu_G(\rho'_s) - \rho'_0\mu_G(\rho'_0) - f_G(\rho'_s) + f_G(\rho'_0)] \end{aligned} \tag{6}$$

where ρ'_s and ρ'_0 are the cobalt cation concentrations in the LCG layer at the boundaries with the extradialytic solution and with the inner DNA solution, respectively. The function f_G is defined as $\partial f_G(\rho')/\partial\rho' = \mu_G(\rho')$.

The assumption (a) gives the relationship;

$$2\pi Rj(R)dt = 2\pi(R-x)(\rho_g - \rho_0)dx, \tag{7}$$

where ρ_0 is the cobalt cation concentration in the inner DNA solution. From (6) and (7), we have a differential equation;

$$\frac{dx}{dt} = K \frac{1}{(R-x)\ln\dfrac{R}{R-x}} \tag{8}$$

with

$$K = \frac{A}{\rho_g - \rho_0} \tag{9}$$

In terms of the scaled distance and the scaled time, eq.(8) is rewritten as

$$\frac{d\tilde{x}}{d\tilde{t}} = K \frac{1}{(1-\tilde{x})\ln\dfrac{1}{1-\tilde{x}}} \tag{10}$$

Finally, we obtain the solution (1) of the above equation.

2.4 Results

Immersion of DNA aqueous borate solution sandwiched between two circular glass plates into the concentrated cobalt chloride solution induced gelation and shrinking of the DNA gel. Figure 7 (a) showed the time course of the shrinking ratio γ (*t*) in thickness and γ'(*t*) in cross-sectional area of the DNA gel with initial radius of *R* = 9 mm. The thickness of DNA aqueous solution decreased with immersion time *t*, whereas the cross-section virtually unchanged after initial slight decrease. The gelation of DNA aqueous solution was completed within 240 min, while the shrinking process still continued. The time course of shrinking ratio in thickness decayed exponentially, and achieved the equilibrium state after around 2 day immersion, as shown in Figure 7 (b). At the equilibrium state, the size reduction by gelation of DNA aqueous borate solution was 35% in thickness, 5% in cross-sectional area, and 38% in volume.

Time course of the normalized DNA weight fraction $W_i(t)=w_i(t)/w_0$ in each section of DNA LCG, S_i, (i=1 to 4) is shown in Figure 8, where $w_i(t)$ and w_0 are the DNA weight fraction of each section, S_1 through S_4, at immersion time t and the overall DNA weight fraction of the intradialytic solution before the dialysis, respectively. The arrows indicate the times when gelation begins at S2 and S3. With increasing t, $W_1(t)$, $W_2(t)$, and $W_3(t)$ for the LCG layer increased after gelation began, whereas $W_4(t)$ in the inner amorphous layer S_4 decreased. Therefore, DNA molecules are concentrated into the LCG layer by liquid crystalline gelation to form DNA weight fraction gradient.

The time course of concentration of cobalt cations C_{Co} is shown in Figure 9. C_{Co} in the LCG layer increased quickly to reach the critical value for forming LCG at the initial stage and then further increased proportionally with immersion time. By extrapolating the value of C_{Co} to t=0, the cobalt concentration required to form LCG is determined as ρ_g =6.8×10^{-5} mol/g. On the other hand, C_{Co} in the inner solution increased proportionally with t, and the slope agreed with that in the LCG layer.

Figure 10 shows the time courses of birefringence Δn (a) and turbidity τ (b) of DNA solution or LCG observed at an outermost point (r = 7.0 mm (0.5mm from the circumference of glass plates)) of the LCG layer. Δn and τ increased quickly at the very early stage of immersion. The steepest slope for Δn and τ is observed around 10 min. After 50 min τ was roughly constant whereas Δn still increased slightly with t.

Figure 11 shows the time course of the distance x between the gel front line and the circumference of LCG for various R. The distance x seems to increase proportionally to the square root of immersion time, irrespective of R. The liquid crystal front did not reach the center of the gel even after a week, but stopped around 0.6R. Figure 12 shows the scaled plot corresponding to the theoretical equation (1). Though a master

curve is obtained irrespective of gel size, the linear relationship expected from Eq. (1) is observed only at the early stage $\tilde{t} \leq 1300\,\mathrm{s/cm^2}$, but a constant line is observed at the later stage. The intersection point of the two lines should denote the completion of LCG formation. The whole curve is characterized by the coefficient *K* given by the initial slope, the scaled distance characterized by the quantity $\tilde{y}_e$ and the scaled time $\tilde{t}_e$ for the completion of LCG formation. From the value of the initial slope and the expression (2), we have the diffusion coefficient of cobalt cations in the LCG layer as $\overline{D}_{\mathrm{Co}} = 5.1\times10^{-6}\,\mathrm{cm^2/s}$. This value is smaller than the diffusion coefficient estimated by Einstein-Stokes equation for cobalt cations in pure water at 20°C of $3.6\times10^{-5}\,\mathrm{cm^2/s}$. The difference between the two values could be attributed to the effect of friction induced by DNA network of gel. The same degree of diffusion coefficient decreasing due to polymer network of gel was obtained for the calcium cation diffusion in the curdlan LCG layer (26). Figure 13 shows the scaled time course for the samples with various cobalt chloride concentrations, and Fig. 14 shows cobalt chloride concentration (C_{co}) dependence of these parameters. *K* and $\tilde{y}_e$ increase and $\tilde{t}_e$ decreases with increasing C_{co} and all of them saturate at high C_{co}. Figures 15 and 16 show the corresponding ones for DNA concentration (C_{DNA}) dependence. Dependence of these quantities on C_{DNA} is quite weak.

2.5 Discussion

To elucidate the dynamics of dialysis-induced liquid crystalline gelation, in this study we developed “solution-sandwich method”. Cross-linking of DNA molecules at the

circumference of the cover glasses allowed us to prepare a thin membrane just after the immersion of the sandwiched DNA solution into aqueous cobalt chloride, and the dialysis through the circumference induced liquid crystalline gelation with cylindrical symmetry. The phenomena observed during the process are (I) the gelation of DNA aqueous solution, (II) the shrinking of the DNA gel, (III) the orientation of DNA molecules, and (IV) the formation of DNA weight fraction gradient. As shown in Fig. 7, the shrinking of DNA solution occurred anisotropically: The thickness decreased by 35 %, whereas the cross-sectional area decreased only by 1 %. The shrinking is attributed to syneresis of DNA LCG. High wettability between DNA solution and the cover glasses and adhesion of DNA LCG to the glasses prevents from large change in cross-sectional area. The shrinking resulted in enhancement of DNA concentration in LCG layer. The normalized DNA concentration W_4 at the inner solution of S4 decreases with immersion time t and reaches a constant of W_4~0.7 (w_4=0.66wt%), as shown in Fig. 8. On the other hand, W_1, W_2 and W_3, at the LCG layers of S1, S2 and S3 increased with t after the gelation. Note that the initial decrease of DNA concentrations W_2 and W_3 corresponds to the period when the parts S2 and S3 are solution state (before gelation). The DNA concentration gradient is attributed to condensation of DNA at LCG layer associated with the gel shrinking. The corresponding time course of cobalt concentration is shown in Fig. 9. The quick increase of cobalt concentration at the outermost LCG layer indicates LCG formation at the initial state. The cobalt concentration required to form LCG, ρ_g =6.8×10^{-5} mol/g, determined by extrapolating the value of C_{Co} to t=0 corresponds to the molar ratio r_M=[base pair]:[Co^{2+}] of 1:4. The binding sites of DNA molecules for cobalt cations per base pair are two phosphate groups of the double helical DNA backbone and the

interstices of the base pair, as well as the inner core of the helices to form M-form (13, 42-43). Therefore, the r_M estimated from the experiment indicates almost full occupancy of the binding sites of DNA. The simultaneous increase of the birefringence Δn and the turbidity τ as shown in Fig. 10 indicates that the liquid crystal formation and gel network formation occurs at the same time, and the liquid crystallization (orientation of DNA) is coupled with the gelation (intermolecular cross-linking). On the other hand, the broadness of the time range for the change of τ is much larger than that of Δn, and τ increases further even after LCG formation. These behaviors could be attributed to local shrinking and the resultant increase in inhomogeneity.

As shown in Fig. 12, scaling the LCG layer width x by R and the immersion time t by R^2 makes all the data sit on a master curve. This type of scaling suggests the LCG growth behavior is governed by diffusion. The linear relationship in the initial stage shows the moving boundary picture for the LCG formation is valid at least in the initial stage. However, the parallel increase of cobalt concentration at the inner solution and LCG layer after the initial increase shown by Fig. 9 requires a modification of the assumptions (a) and (b) which hold for the process forming curdlan LCG (26), as follows. (a')A definite number of cobalt cations flowing into the inner polymer solution are used up to produce the LCG layer and the remaining cobalt cations come to be mixed in the inner polymer solution. (b')The LCG layer captures the cobalt cations flowing from the extradialytic solution into the inner polymer solution, and the amount of the captured cobalt cations per unit volume of LCG layer is a constant independent of time and position.

Let us reconstruct the moving boundary picture on the basis of the new assumptions (a') and (b'). From the assumption (b'), we could generalize Eq.(5) as

$$\mathrm{div}\vec{j} = -\frac{1}{r}\frac{\partial rj}{\partial r} = -q \tag{11}$$

where q is the cobalt cation number captured per unit LCG volume per unit time and is a constant independent of time and position. The solution of Eq.(11) is obtained as

$$j(r) = \frac{1}{2}qr + \frac{C'}{r} \tag{12}$$

where C' is the integral constant. The number of the cobalt cations captured by the LCG layer per unit time is given by

$$Q(t) = 2\pi Rj(R) - 2\pi(R-x)\,j(R-x) = [\pi R^2 - \pi(R-x)^2]q \tag{13}$$

Then, the captured cobalt cation number per unit volume per unit time is verified to be $Q(t)/[\pi R^2 - \pi(R-x)^2] = q$. Denoting the cobalt cation concentration at time t and position r by $\rho'(r,t)$ and using Eqs.(3) , (4) and (12), we have

$$k\frac{\partial \mu_G(\rho'(r,t))}{\partial r}\rho'(r,t) = \frac{1}{2}qr + \frac{C'}{r} \tag{14}$$

Integrating both sides of the above equation from $r = R-x$ to $r = R$, we have

$$k[g_G(\rho'_s) - g_G(\rho'_0(t))] = \frac{1}{4}q[R^2 - (R-x)^2] + C'\ln\frac{R}{R-x} \tag{15}$$

where

$$g_G(\rho) = \rho\mu_G(\rho) - f_G(\rho) \tag{16}$$

and $\rho'_0(t)$ is the cobalt concentration in the LCG layer at the boundary with the inner DNA solution for the time t. Then, we have the integral constant C' as

$$C' = \frac{k[g_G(\rho'_s) - g_G(\rho'_0(t))] - \frac{1}{4}q[R^2 - (R-x)^2]}{\ln\frac{R}{R-x}} \tag{17}$$

To simplify the above expression, we use the fact that g_G stands for the osmotic

pressure of cobalt cations in the LCG layer. Let us assume the osmotic pressure is balanced at the boundaries between the LCG layer and the extradialytic solution and between the LCG layer and the inner DNA solution, and adopt the ideal gas picture for cobalt cations in the solutions. Then, we have

$$g(\rho_s') \cong k_B T \rho_s \tag{18}$$

and

$$g(\rho_0') \cong k_B T \rho_0 \tag{19}$$

where T is the temperature and k_B is the Boltzmann constant. Using these expressions, C' is rewritten as

$$C' = \frac{k k_B T(\rho_s - \rho_0(t)) - \frac{1}{4} q[R^2 - (R-x)^2]}{\ln \frac{R}{R-x}} \tag{20}$$

The presence of the critical value ρ_g of the cobalt concentration to form the LCG layer at the initial stage enables us to generalize Eq.(7) on the basis of the assumption (a') as follows.

$$\begin{aligned} 2\pi(R-x)\, j(R-x)dt = {} & 2\pi(R-x)(\rho_g - \rho_0(t))dx \\ & + \pi(R-x-dx)^2[\rho_0(t+dt) - \rho_0(t)] \end{aligned} \tag{21}$$

Hence, we have

$$j(R-x) = (\rho_g - \rho_0(t))\frac{dx}{dt} + \frac{1}{2}(R-x)\frac{d\rho_0(t)}{dt} \tag{22}$$

The parallel increase shown by Fig. 4 requires the relationship

$$\frac{d\rho_0}{dt} = q \tag{23}$$

From the initial condition $\rho_0(0) = 0$, we have

$$\rho_0 = qt \tag{24}$$

From Eqs.(12), (20) and (24), Eq.(22) is rewritten as

$$\frac{kk_B T(\rho_s - qt) - \frac{1}{4}q[R^2 - (R-x)^2]}{(R-x)\ln\frac{R}{R-x}} = (\rho_g - qt)\frac{dx}{dt} \tag{25}$$

The scaling behavior shown in Fig. 12 requires that the R dependence of Eq.(25) disappears by the scaling $\tilde{t} = t/R^2$ and $\tilde{x} = x/R$. Hence, q should be expressed as $q = \tilde{q}/R^2$, where $\tilde{q}$ is a constant independent of R. In terms of the scaled quantities, we obtain that

$$\frac{K'}{(1-\tilde{x})\ln\frac{1}{1-\tilde{x}}} = \frac{d\tilde{x}}{d\tilde{t}} \tag{26}$$

with

$$K' = \frac{kk_B T(\rho_s - \tilde{q}\tilde{t}) - \frac{1}{4}\tilde{q}\tilde{x}(2-\tilde{x})}{(\rho_g - \tilde{q}\tilde{t})} = \frac{kk_B T\rho_s - \tilde{q}[kk_B T\tilde{t} + \frac{1}{4}\tilde{x}(2-\tilde{x})]}{(\rho_g - \tilde{q}\tilde{t})}$$
$$= \frac{kk_B T\rho_s}{\rho_g}\Delta K(\tilde{x},\tilde{t}) \tag{27}$$

$$\Delta K(\tilde{x},\tilde{t}) = \frac{1 - \frac{\tilde{q}}{\rho_s}[\tilde{t} + \frac{1}{4}\frac{1}{kk_B T}\tilde{x}(2-\tilde{x})]}{1 - \frac{\tilde{q}\tilde{t}}{\rho_g}}$$

(28)

The linear behavior between $\tilde{y}$ and $\tilde{t}$ in the early stage of the experimental results suggests that the $\tilde{x}$- and $\tilde{t}$- dependence of the correction factor ΔK is quite weak and K' is regarded as a constant. Then, K' is the slope of the linear behavior and increases with increasing cobalt cation concentration in the extradialytic solution.

This suggestion is consistent with the slope increase behavior shown in Fig. 13 or Fig. 14(a). The saturation behavior in Fig. 14 may attribute to the presence of the maximum osmotic pressure π_{MAX} for cobalt cations or the maximum value of ρ_s'. When ρ_s is large, the balance equation (18) is modified as

$$\pi_{MAX} + \sigma \cong k_B T \rho_s \tag{29}$$

where σ is the surface tension of the LCG. In this case, the expression (27) is modified as

$$K' = \frac{\pi_{MAX} - \tilde{q}[kk_B T\tilde{t} + \frac{1}{4}\tilde{x}(2-\tilde{x})]}{(\rho_g - \tilde{q}\tilde{t})} \tag{30}$$

Then, K' is independent of ρ_s.

Figures 15 and 16 show that the scaled LCG width (characterized by the value of $\tilde{y}_e$) at the LCG formation completion time and the boundary motion, $x = x(t)$, are independent of the DNA concentration. The DNA concentration independence of $\tilde{y}_e$ is attributed to the one body problem of DNA molecule. The circumstance change, e.g. the pH change of the DNA solution in the course of dialysis, may induce the DNA molecule condition change. In fact, the phase diagram reported in the preceding paper (15) predicts that DNA forms LCG at cobalt chloride concentration of extradialytic solution of 0.1M at the DNA concentration of 0.66wt% which is the final DNA concentration at the inner "solution" (S4) shown in Fig. 8. This apparent contradiction could attribute to the DNA circumstance difference. The condition change could prohibit the LCG formation and give the value of $\tilde{y}_e$ smaller than the

maximum value 0.25 and independent of C_{DNA}. Under the non-LCG-growth circumstance, the DNA molecules form only fragile amorphous gel. Thus, the growth process of DNA LCG consists of two dynamics: cobalt cation diffusion limited process at the early stage and the DNA circumstance change limited process at the later stage. The DNA concentration independence of the boundary motion suggests the DNA concentration independence of the critical value ρ_g. The reason for the independence is speculated as follows. When the DNA LCG is produced by the cobalt cation flow, all of DNA molecules in the DNA solution are not used but a part of them is used. The amount of DNA molecules required for the "first" DNA LCG formation does not depend on the DNA concentration in the prepared DNA solution. The DNA LCG layer gradually matures, capturing the cobalt cations and importing DNA molecules contained by itself in the solution state. The time courses of turbidity and birefringence shown in Fig. 10 are consistent with this speculation.

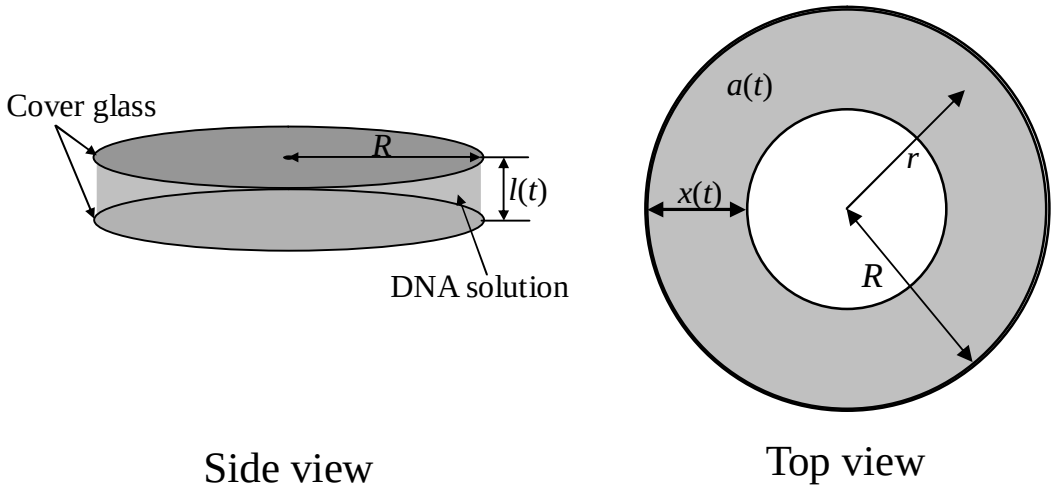

Figure 6. Schematic illustration of the experimental setup.

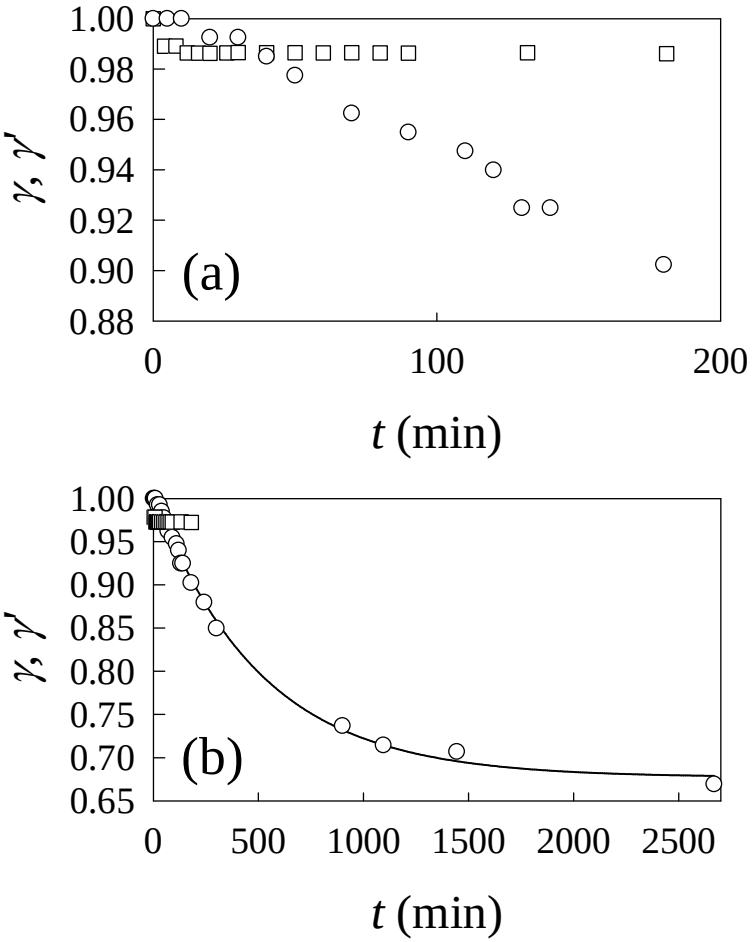

Figure 7. Time course of shrinking ratios $\gamma(t)$ in thickness (circle) and $\gamma'(t)$ in cross-section (square) of the DNA gel with R = 9mm in early stage (a) and whole stage (b).

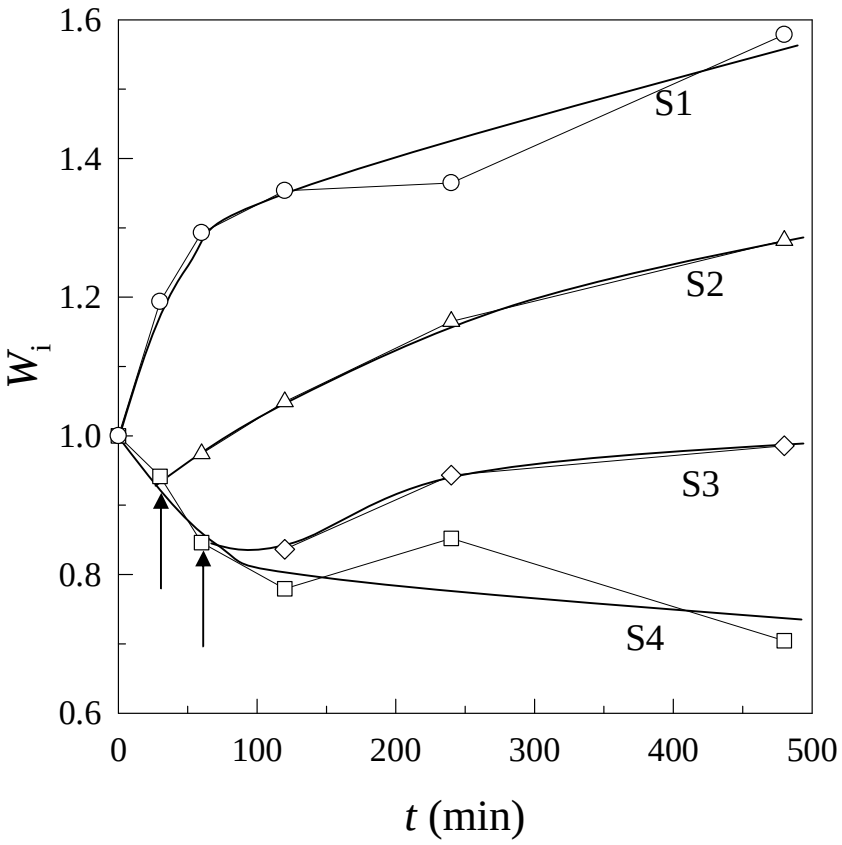

Figure 8. Time course of normalized DNA weight fraction of the strips excised from different circumferential layers of the sample with R = 9 mm; S1 (7 mm < r < 9 mm, circle), S2 (5 mm < r < 7 mm, triangle), S3 (3 mm < r < 5 mm, diamond), and S4 (inner solution region, square), respectively, where r is the distance from the center. The arrows indicate the times when gelation begins in S2 and S3.

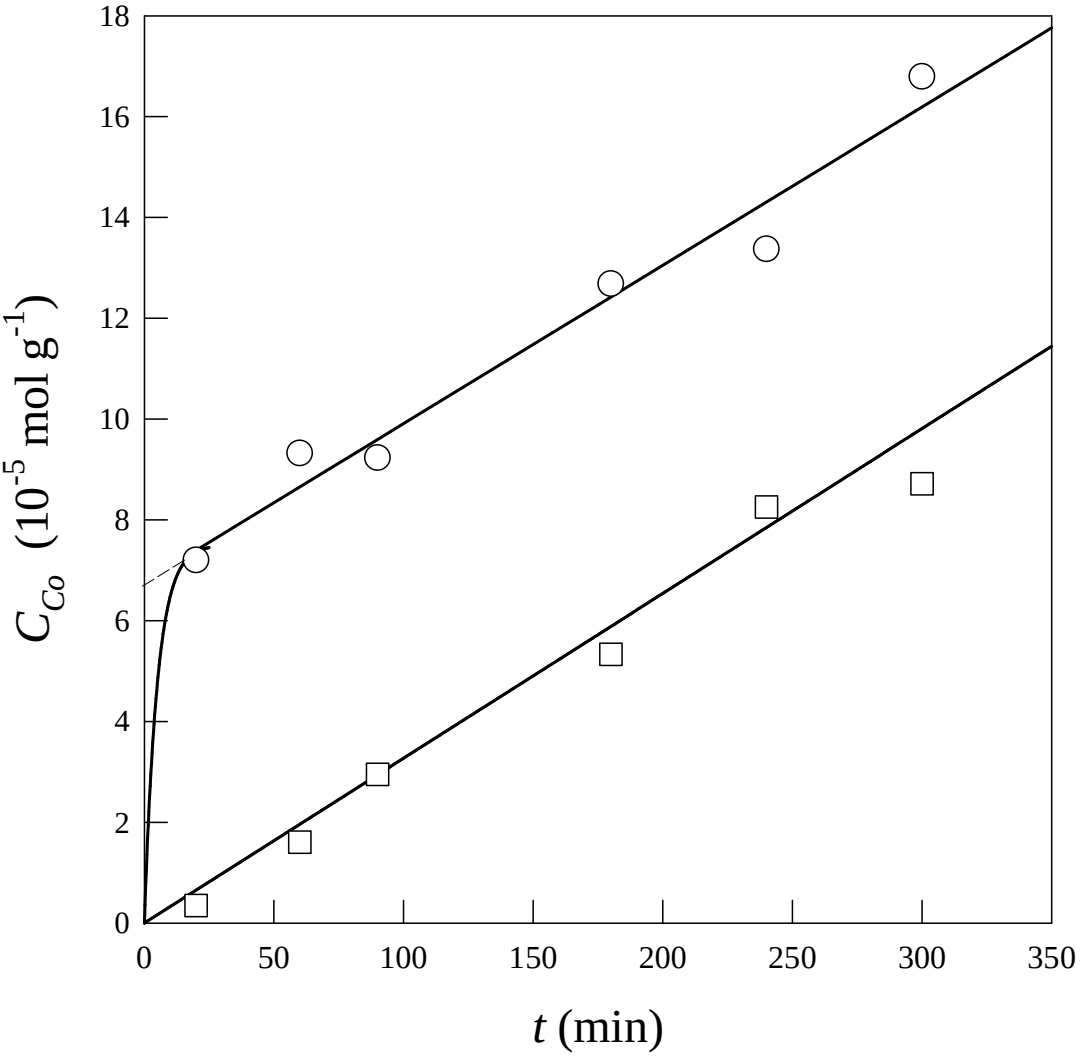

Figure 9. Time course of cobalt concentration at outer LCG layer (circle) and inner solution (square) for the sample with R = 9 mm.

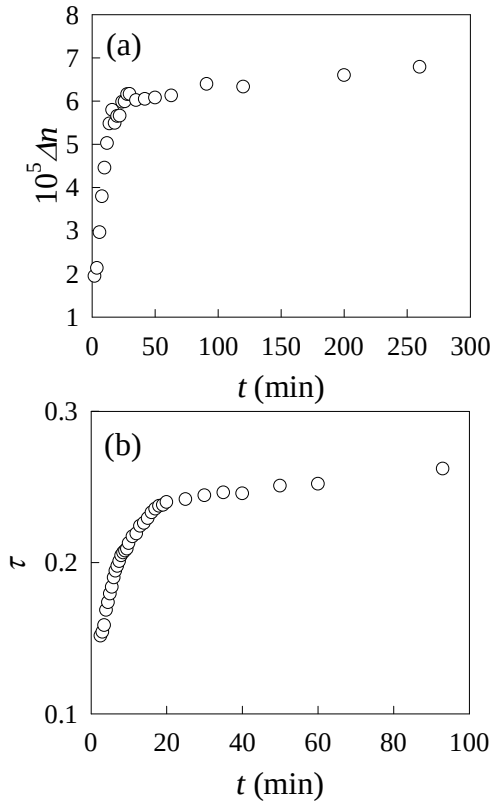

Figure 10. Time course of birefringence (a) and turbidity (b) observed at the outmost layer of DNA LCG of the sample with R = 7.5 mm.

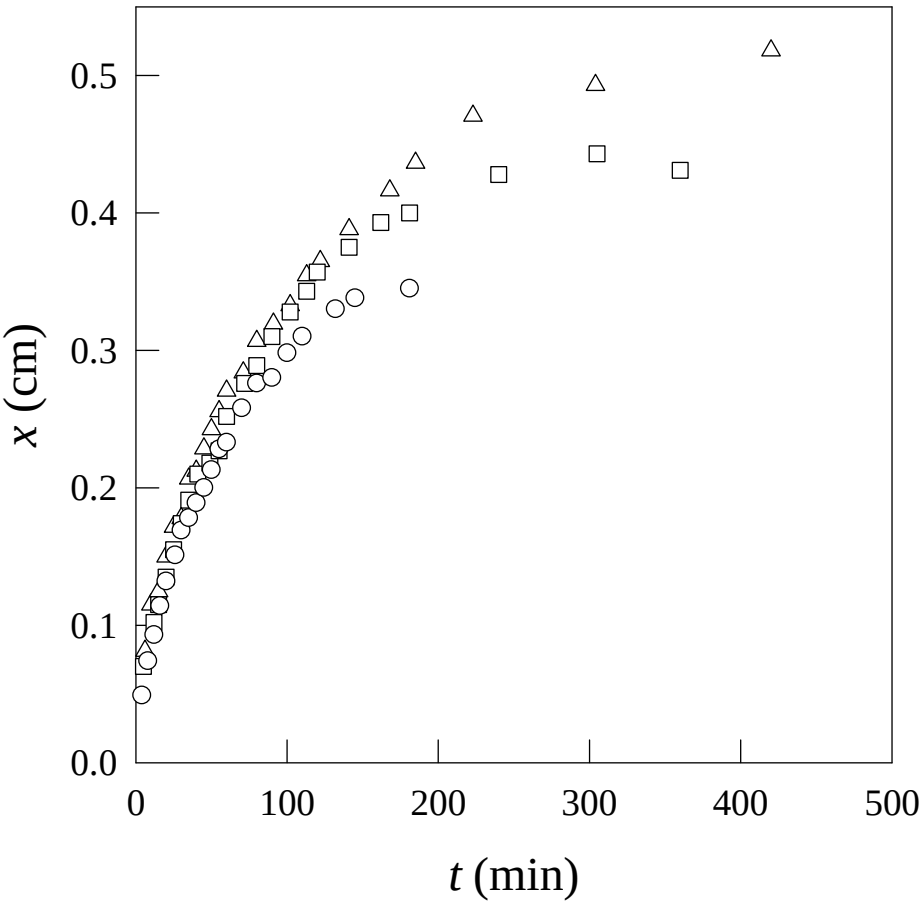

Figure 11. Time course of the width of LCG layer *x* versus immersion time *t* (min) for the samples with *R* = 6 (circle), 7.5 (triangle), and 9 mm (square).

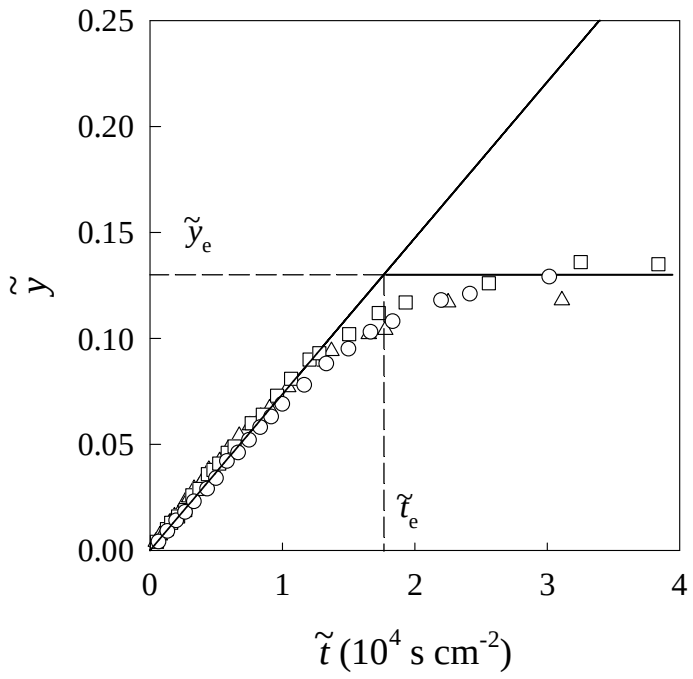

Figure 12. LCG formation process expressed with the function $\tilde{y}(\tilde{x})$ against the scaled time $\tilde{t}$ for the samples with different *R*. The symbols are the same as in Figure 11.

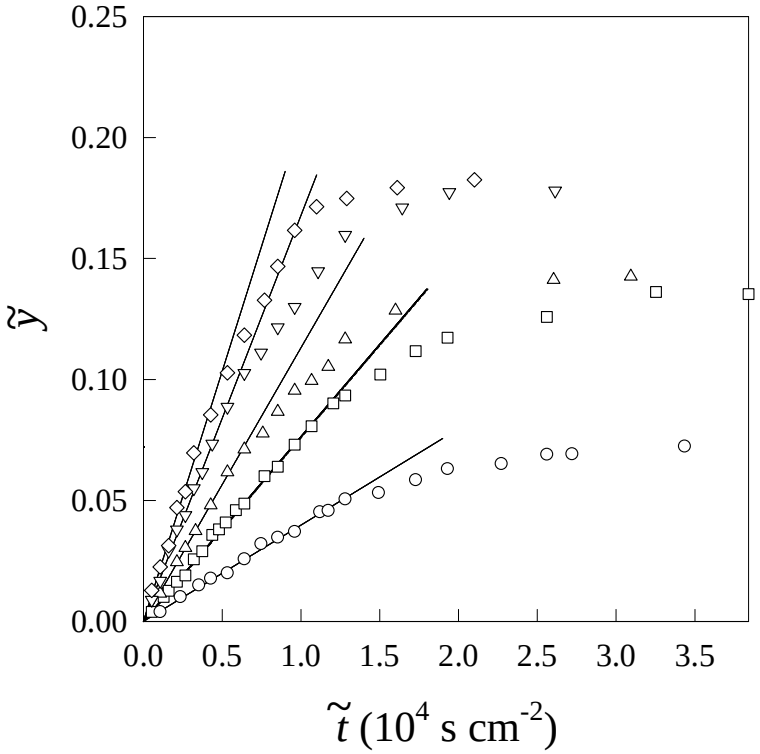

Figure 13. LCG formation process expressed with the function $\tilde{y}(\tilde{x})$ against the scaled time $\tilde{t}$ for the samples with 1wt % DNA concentration and various cobalt chloride concentrations in the extradialytic solution; 50 mM (circle), 100mM (square), 200 mM (triangle), 400mM (triangle down), and 800mM (diamond) at R = 9 mm

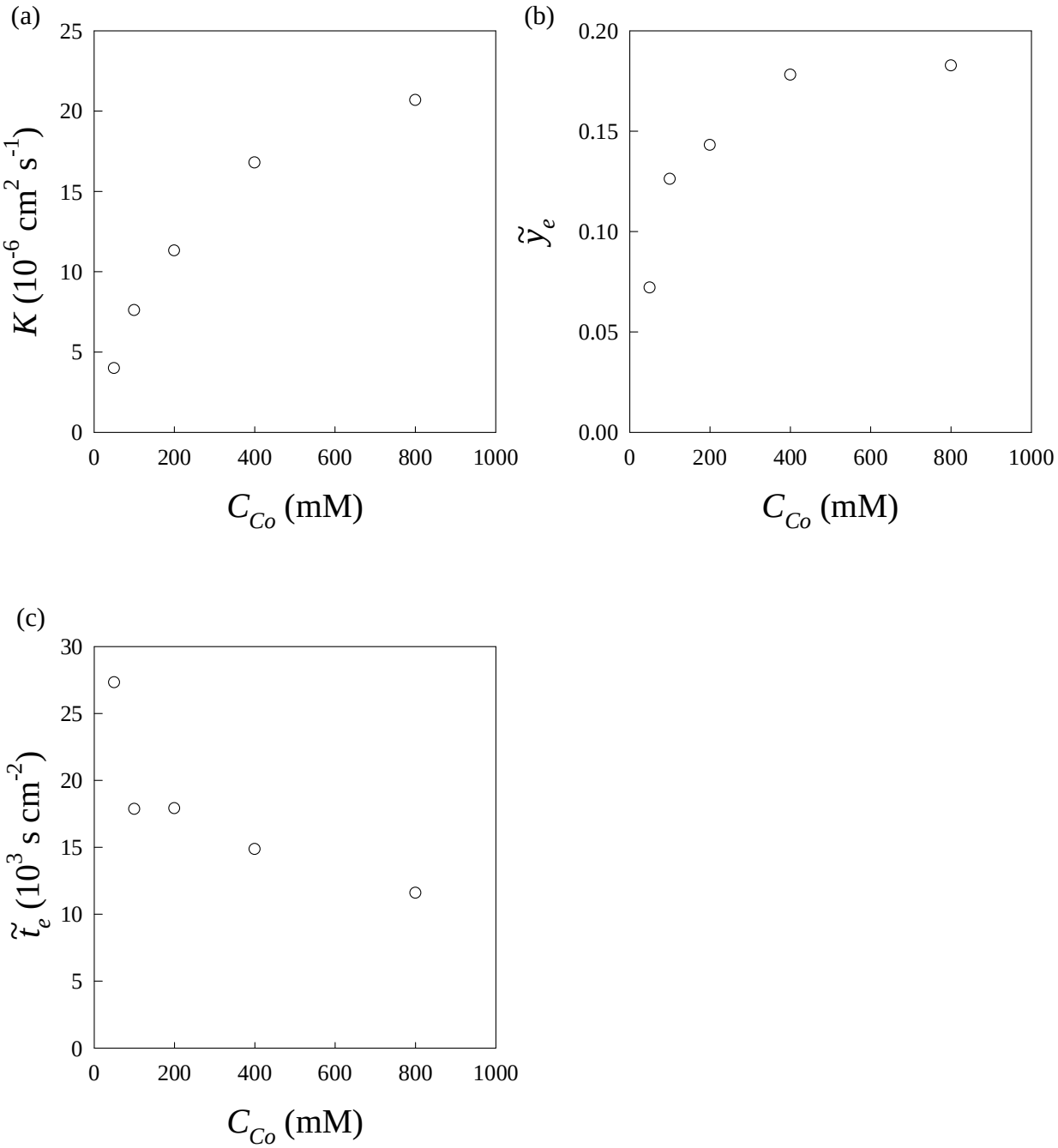

Figure 14. Cobalt chloride concentration (in the extradialytic solution) dependence of (a) the coefficient *K* in eq 1, (b) the scaled distanve of LCG layer, and (c) scaled time for LCG completion at 1 wt % DNA

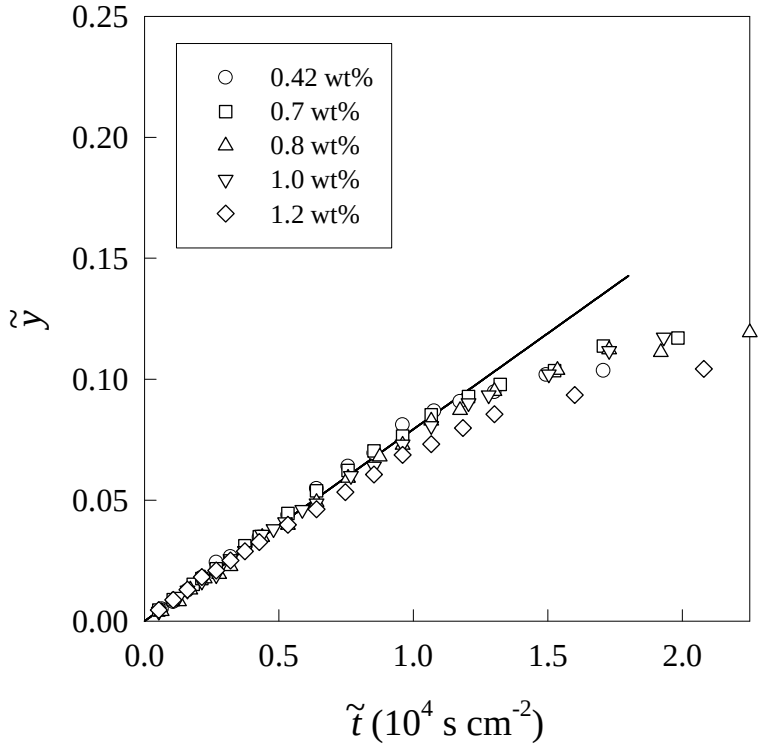

Figure 15. LCG formation process expressed with the function $\tilde{y}(\tilde{x})$ against the scaled time $\tilde{t}$ for the samples with 100mM cobalt chloride in the extradialytic solution and various DNA concentrations of 0.42 wt % (circle), 0.70 wt % (square), 0.80 wt % (triangle up), 1.00 wt % (triangle down), and 1.20 wt % (diamond) at R = 9 mm.

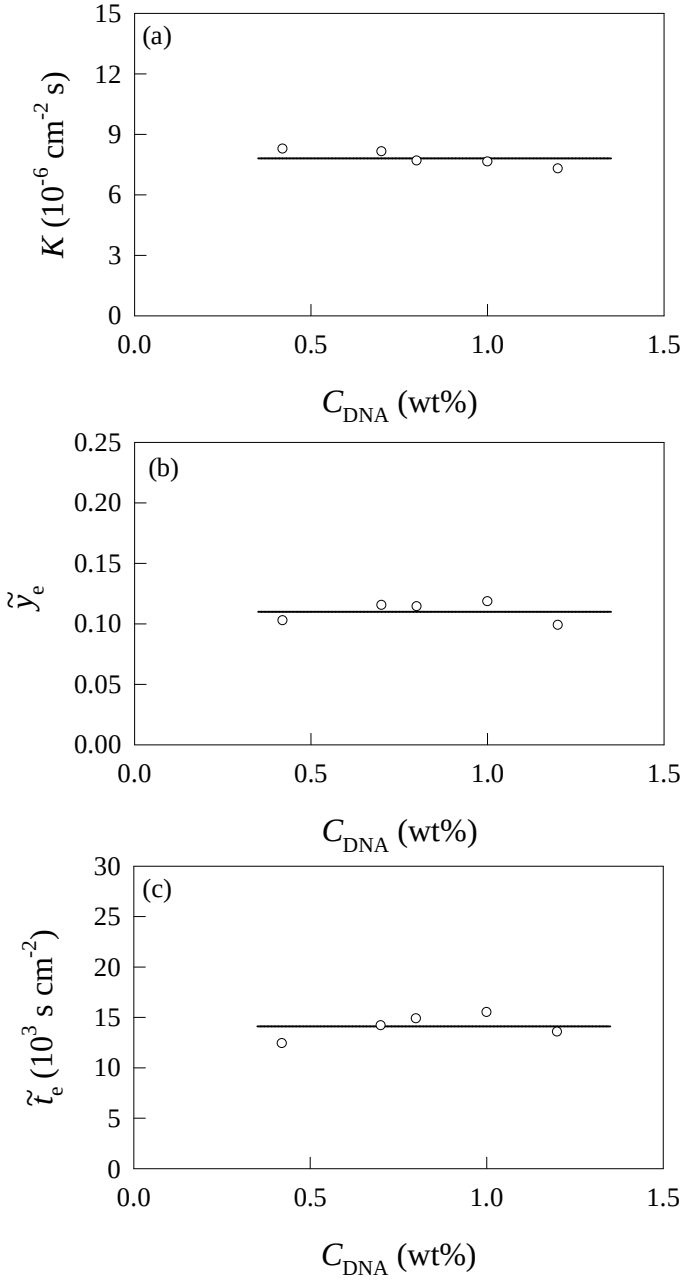

Figure 16. DNA concentration dependence of (a) the coefficient *K* in eq 1, (b) the scaled width of LCG layer, and (c) the scaled time for LCG completion at 100mM cobalt chloride in the extradialytic solution.

Chapter 3

Adsorption Kinetics of Carcinogens to DNA Liquid Crystalline Gel Beads

3.1 Introduction

Recently, global air and water pollution by toxic chemical agents has grown into a serious problem. Particularly, halogenated compounds having aromatic planner groups such as polychlorinated biphenyl, dioxin and benzopyrene, result in mutation and endocrine disruption through intercalation into major grooves and interstices between base pairs of DNA double helices (4,14-15). This fact suggests that materials consisting of DNA or DNA composites can be utilized as the most efficient adsorbents for such toxic agents. In Chapter 2, we developed a DNA liquid crystalline gel (LCG) beads prepared from DNA concentrated solutions by using insolubilization reaction method in multivalent metal cation solutions, and found that they can adsorb carcinogens having planer aromatic groups. Therefore, this new material is expected to be utilized as an intelligent probe and an adsorbent of toxic agents with the advantage of having anisotropic optical properties and a high capacity to hold solvents.

In this chapter, to describe the experimental data and to analyze the adsorption behavior, we have developed a theory for the adsorption kinetics of carcinogen to DNA LCG beads by using nonequilibrium thermodynamics with simple assumptions. To compare the theoretical and experimental results, we found that the adsorption process at an early stage is explained by diffusion limited binding of the carcinogen molecules

to DNA beads, and that the time range of the early stage depends on the solubility, while the process at later stage depends on the balance of the numbers of adsorption sites and carcinogen molecules.

3.2 Experiments

Sodium-type double-stranded DNA extracted and purified from salmon milt was provided from Japan Chemical Feed Co. Ltd. The nominal average base pair examined by electrophoresis was 10kbp. Cobalt chloride and sodium tetraborate were purchased from Wako Pure Chemicals. MilliQ water was used as solvent. A desired amount of DNA was dissolved in 20mM sodium tetraborate aqueous solution at 1.0wt%. In order to prepare DNA LCG beads, the DNA solution was poured drop by drop into cobalt chloride solutions with various concentrations in the range between 50-1000 mM at 25^{o}C. The interfacial layer formed by the initial reaction played the role of dialysis tubing, and the dialysis from the spherical surface was performed to make small beads with almost the same diameter of 2-3 mm. Biphenyl (BP) and acridine orange (AO) purchased from Wako Chemicals were used.

For the measurements of adsorption of AO by DNA LCG beads, 0.3 g of the beads was immersed into 10ml of aqueous solution of AO at 13μg/mL, which was gently stirred and thermally controlled at 25^{o}C. The optical density (A_{495}) of the AO solution was measured at wavelength λ = 495nm as a function of immersion time t. The concentration of AO in the solution, C_{AO}, was calculated from a calibration equation $C_{AO} = 14.14 \times A_{495}$ (μg/cm^3) obtained by standard solutions with known concentrations.

For the measurements of adsorption of biphenyl by the DNA LCG beads, 1.2 g of the beads was immersed into 10mL of aqueous solution saturated by biphenyl (6.3 μg/cm^3),

which was gently stirred and thermally controlled at 25°C. The optical density (A_{250}) of the biphenyl solution was measured at wavelength λ = 250nm as a function of immersion time *t*. The concentration of biphenyl in the solution, C_{BP}, was calculated from a calibration equation $C_{BP} = 9.86 \times A_{250}$ (μg/cm^3).

3.3 Theoretical Analysis

Let's consider a DNA gel bead with radius *R* in solution of carcinogen molecules with volume *V*. To discuss the carcinogen molecule adsorption behavior, we adopt the following assumptions. (A) All carcinogen molecules flowing into the beads are used up to produce the adsorbed layer in which the DNA gel adsorbs carcinogen molecules up to the maximum density; all the adsorption sites are saturated with carcinogen molecules. (B) In the adsorbed layer, carcinogen molecules are not captured. These assumptions make us to pay attention to the boundary between the adsorbed layer and the non-adsorbed part of the bead, in which no carcinogen molecules are adsorbed. Then, the adsorption dynamics can be illustrated in terms of the "boundary-moving dynamics". The moving boundary picture for illustrating diffusion and "adsorption" process was proposed to analyze the curdlan liquid-crystalline gel formation (26). It is valid when the carcinogen molecules flowing into the gel are adsorbed instantly or the carcinogen molecules penetrate the non-adsorbed layer hardly whereas the adsorbed layer relatively easily.

Since the adsorbed behavior is spherically symmetric, the position of the boundary is expressed by the distance r from the bead center. In the spherical cell region, $R \geq x \geq r$, where x is the distance from the center, all the adsorption sites are occupied by carcinogen molecules (the adsorbed layer) and in the sphere region,

$r \geq x \geq 0$, all the adsorption sites are empty. The illustration of the model system and the notations are given in Figure 17. n_0, n_f, ρ_f, and $n(t)$ denote the number of carcinogen molecules in the dispersing solution at the initial state, the maximum number of carcinogen molecules that the DNA LCG bead is capable to adsorb, the maximum number density of carcinogen molecules adsorbed to the bead, and the number of carcinogen molecules adsorbed to the bead at immersion time *t*, respectively. The time development of the boundary $r = r(t)$ gives the time course of $n(t)$.

Since the flux of carcinogen in the adsorbed layer is spherically symmetric, the flux density vector of carcinogen flowing into the inner core is given by

$$\vec{J} = -J(x)\vec{e}_r$$
$$J(x) = k\rho(x)\frac{\partial \mu(x)}{\partial x} \qquad (1)$$

where $\vec{e}_r$ is the unit vector along the radial direction of the gel bead, k is the mobility of carcinogen molecules, and $\rho(x)$ and $\mu(x)$ are the number density and the chemical potential of carcinogen molecules at point *x*, respectively. In the adsorbed layer, $R \geq x \geq r$, the assumptions give the quasi-steady state flow;

$$\mathrm{div}\vec{J} = -\frac{1}{x^2}\frac{\partial x^2 J(x)}{\partial x} = 0 \qquad (2)$$

The solution of equation (2) is given by

$$J(x) = \frac{C}{x^2} \qquad (3)$$

where *C* is the integral constant. From equations (1) and (3), we have

$$k\rho(x)\frac{\partial \mu(x)}{\partial x} = \frac{C}{x^2} \qquad (4)$$

Integrating both sides of the above equation from $x = r$ to $x = R$, we have

$$k\{\rho(R)\mu(R) - \rho(r)\mu(r) - f(\rho(R)) + f(\rho(r))\} = C\frac{R-r}{Rr} \qquad (5)$$

The left hand side of equation (5) is rewritten as

$$k\{\rho(R)\mu(R)-\rho(r)\mu(r)-f(\rho(R))+f(\rho(r))\}\equiv k(g(R)-g(r)) \qquad (6)$$

Here, $f(\rho)$ is the free energy of carcinogen molecules per unit volume; $\mu=\partial f/\partial\rho$. The osmotic pressure of carcinogen molecules is expressed as

$$g(\rho)=\rho\mu-f(\rho) \qquad (7)$$

From equations (5), (6) and (7), the constant C is expressed as

$$C=\frac{kRr}{R-r}(g(R)-g(r)) \qquad (8)$$

The number of adsorbed carcinogen molecules per unit time is given by

$$\frac{dn}{dt}=4\pi R^2 J(R) \qquad (9)$$

From equations (3) and (8), the right hand side of equation (9) is rewritten as

$$4\pi R^2 J(R)=\frac{4\pi kRr}{R-r}[g(R)-g(r)] \qquad (10)$$

Since the carcinogen molecules are not adsorbed to the inner core of the bead ($x\le r$), the osmotic pressure of the carcinogen molecules is 0 there. On the surface of the bead, the osmotic pressure of the carcinogen molecules is equal to that of solvent. From the ideal gas approximation, we have

$$g(R)\cong k_B T\rho_s(t) \qquad (11)$$

where $\rho_s(t)$ is the number density of carcinogen molecules in solvent at time t. Therefore, equation (9) is rewritten as

$$4\pi R^2 J(R)\cong\frac{4\pi kRr}{R-r}k_B T\rho_s(t) \qquad (12)$$

On the other hand, the number of adsorbed carcinogen molecules can be related to the boundary position $r(t)$ as

$$n(t)=\left[\frac{4}{3}\pi R^3-\frac{4}{3}\pi r^3\right]\rho_f \qquad (13)$$

Using the spherical shape condition $(4/3)\pi R^3 \rho_f = n_f$, we have

$$r(t) = R\left(1 - \frac{n(t)}{n_f}\right)^{1/3} \tag{14}$$

From the mass conservation law

$$V\rho_s(t) + n(t) = n_0 \tag{15}$$

we have

$$\rho_s(t) = \frac{n_0 - n(t)}{V} \tag{16}$$

Thus, from equations (12), (14) and (16), we obtain

$$4\pi R^2 J(R) \cong \frac{4\pi k k_B T R\left(1 - n(t)/n_f\right)^{1/3}}{1 - \left(1 - n(t)/n_f\right)^{1/3}} \frac{n_0 - n(t)}{V} \tag{17}$$

From equations (9) and (17), the time development equation for *n* is given by

$$\frac{dn}{dt} = \frac{4\pi k k_B T R}{V} \frac{\left(1 - n(t)/n_f\right)^{1/3}\left(n_0 - n(t)\right)}{1 - \left(1 - n(t)/n_f\right)^{1/3}} \tag{18}$$

Equation (18) is rewritten with a scaled number of adsorbed carcinogen molecules, $\tilde{n} = n/n_f$, and a scaled immersion time, $\tilde{t} = t/\tau_0$ as

$$\frac{d\tilde{n}}{d\tilde{t}} = \frac{\left(1 - \tilde{n}\right)^{1/3}\left(\tilde{n}_0 - \tilde{n}\right)}{1 - \left(1 - \tilde{n}\right)^{1/3}} \tag{19}$$

Here note that $\tau_0 = V/(4\pi k k_B T R)$ and $\tilde{n}_0 = n_0/n_f$. The solution of equation (19) is obtained by using the initial condition $\tilde{n} = 0$ at $\tilde{t} = 0$ as

$$\tilde{t} = \frac{1}{2(\tilde{n}_0 - 1)^{1/3}} \ln \left| \frac{\tilde{n}_0}{\tilde{n}_0 - \tilde{n}} \left(\frac{(1-\tilde{n})^{1/3} + (\tilde{n}_0 - 1)^{1/3}}{1 + (\tilde{n}_0 - 1)^{1/3}} \right)^3 \right|$$
$$+ \frac{\sqrt{3}}{(\tilde{n}_0 - 1)^{1/3}} \left[\tan^{-1} \frac{2 - (\tilde{n}_0 - 1)^{1/3}}{\sqrt{3}(\tilde{n}_0 - 1)^{1/3}} - \tan^{-1} \frac{2(1-\tilde{n})^{1/3} - (\tilde{n}_0 - 1)^{1/3}}{\sqrt{3}(\tilde{n}_0 - 1)^{1/3}} \right]. \quad (20)$$
$$+ \ln \left| \frac{\tilde{n}_0 - \tilde{n}}{\tilde{n}_0} \right|$$

Note that we always choose a real number cubic root of z for the expression of $z^{1/3}$. Introducing a new variable $\tilde{\nu} = n/n_0 = \tilde{n}/\tilde{n}_0$, we have a universal expression for adsorption kinetics of carcinogen molecules to the bead,

$$\tilde{t} = \frac{1}{2(\tilde{n}_0 - 1)^{1/3}} \ln \left| \frac{1}{1-\tilde{\nu}} \left(\frac{\left(\tilde{n}_0^{-1} - \tilde{\nu}\right)^{1/3} + \left(1 - \tilde{n}_0^{-1}\right)^{1/3}}{\tilde{n}_0^{-1/3} + \left(1 - n_0^{-1}\right)^{1/3}} \right) \right|$$
$$+ \frac{\sqrt{3}}{(\tilde{n}_0 - 1)^{1/3}} \left[\tan^{-1} \frac{2 - (\tilde{n}_0 - 1)^{1/3}}{\sqrt{3}(\tilde{n}_0 - 1)^{1/3}} - \tan^{-1} \frac{2\left(\tilde{n}^{-1} - \tilde{\nu}\right)^{1/3} - \left(1 - \tilde{n}_0^{-1}\right)^{1/3}}{\sqrt{3}\left(1 - \tilde{n}_0^{-1}\right)^{1/3}} \right] \quad (21)$$
$$+ \ln \left| 1 - \tilde{\nu} \right|$$

Equation (20) is also represented as

$$\tilde{t} = Q(\tilde{n}) \quad (22)$$

with an integral expression of Q as

$$Q = \int_{(1-\tilde{n})^{1/3}}^{1} \frac{3(1-u)u}{\tilde{n}_0 - 1 + u^3} du \quad (23)$$

If we use a new variable

$$w = 1 - u \quad (24)$$

we have

$$\frac{3(1-u)u}{\tilde{n}_0 - 1 + u^3} = \frac{3w(1-w)}{\tilde{n}_0 - 1 + (1-w)^3} \cong \frac{3w}{\tilde{n}_0 - 1} \quad (25)$$

at the initial stage of the adsorption process; $\tilde{n} \approx 0$ ($u \approx 1$ or $w \approx 0$)

Substitution of equation (25) into equation (23) gives us

$$Q(\tilde{n}) \cong \int_0^{1-(1-\tilde{n})^{1/3}} \frac{3w}{\tilde{n}_0 - 1} dw \cong \frac{1}{6} \frac{1}{\tilde{n}_0 - 1} \tilde{n}^2 \tag{26}$$

Thus, at the initial stage of adsorption, $\tilde{n}$ is proportional to the square root of $\tilde{t}$;

$$\tilde{n} \propto \sqrt{\tilde{t}} \tag{27}$$

The adsorption kinetics at the later stage depends on the value of $\tilde{n}_0$ as follows:

(1) In case of $\tilde{n}_0 > 1$, the adsorption sites in the bead can be saturated with carcinogen molecules and all the carcinogen molecules are not adsorbed. The value of n can reach n_f at a finite completion time t_e of adsorption. Thus, the value of $\tilde{n}$ reach 1 or $(1-\tilde{n})^{1/3}$ vanishes at $t = t_e$. From this condition, equation (23) is rewritten as

$$Q(\tilde{n}) = \int_{(1-\tilde{n})^{1/3}}^{1} \frac{3(1-u)u}{\tilde{n}_0 - 1 + u^3} du \cong \tilde{t}_e - \frac{3}{2} \frac{1}{\tilde{n}_0 - 1} (1-\tilde{n})^{2/3} \tag{28}$$

where the scaled completion time $\tilde{t}_e = t_e / \tau_0$ gives

$$\tilde{t}_e = \int_0^1 \frac{3(1-u)u}{\tilde{n}_0 - 1 + u^3} du \tag{29}$$

Substitution of equation (28) in equation (22) gives

$$\tilde{t}_e - \tilde{t} \cong \frac{3}{2} \frac{1}{\tilde{n}_0 - 1} (1-\tilde{n})^{2/3} \tag{30}$$

Thus, the later process of carcinogen adsorption at $\tilde{n}_0 > 1$ is expressed by the 3/2-th power behavior as

$$1 - \tilde{n} \propto (\tilde{t}_e - \tilde{t})^{3/2} \tag{31}$$

(2) In case of $\tilde{n}_0 < 1$, the carcinogen molecules are completely adsorbed to the bead and some of the adsorption sites in the bead are vacant. n approaches n_0 ; $\tilde{n}$ approaches $\tilde{n}_0$ when $t \to \infty$. Near $u \cong (1-\tilde{n}_0)^{1/3}$ (or large t region), we have approximation expression

$$\frac{3(1-u)u}{\tilde{n}_0 - 1 + u^3} \propto \frac{1}{u - (1-\tilde{n}_0)^{1/3}} \tag{32}$$

Substitution of equation (32) into equation (23) gives us

$$Q(\tilde{n}) \propto \int_{(1-\tilde{n})^{1/3}}^{1} \frac{du}{u - (1-\tilde{n}_0)^{1/3}} = -\ln \frac{(1-\tilde{n})^{1/3} - (1-\tilde{n}_0)^{1/3}}{1 - (1-\tilde{n}_0)^{1/3}} \tag{33}$$

Thus, we obtain

$$\frac{(1-\tilde{n})^{1/3} - (1-\tilde{n}_0)^{1/3}}{1 - (1-\tilde{n}_0)^{1/3}} \cong e^{-t/\alpha\tau_0} \tag{34}$$

where α is a constant. Finally, we have

$$\tilde{n}_0 - \tilde{n} \propto e^{-t/\alpha\tau_0} \tag{35}$$

Therefore, the later process of carcinogen adsorption to the bead at $\tilde{n}_0 < 1$ is expressed by the exponential function.

The results obtained for a single bead also hold for systems composed by many beads with the same radius. For many bead systems, V, n_0, n_f and $n(t)$ are regarded as the volume of the carcinogen molecule solution per one bead, the number of carcinogen molecules per one bead in the dispersing solution at the initial state, the maximum carcinogen molecule number one bead adsorbs and the number of carcinogen molecules adsorbed to one bead at immersion time t, respectively.

3.4 Results

Figure 18(a) and (b) show the adsorption behaviors of AO and BP, respectively, to DNA LCG beads, and Figure 19(a) and (b) are the plots suggested by equation (21): According to the theoretical consideration, the observed adsorption behavior is expressed in terms of scaled number of adsorbed carcinogen molecules to the bead

$\tilde{v}(t) = \frac{\left(\left(C^0_{CM} V_{CM} N_A\right)/M_{CM} - \left(C_{CM}(t) V_{CM} N_A\right)/M_{CM}\right)}{\left(C^0_{CM} V_{CM} N_A\right)/M_{CM}} = \frac{n(t)}{n_0}$ as a function of scaled immersion time $\tilde{t}$, where C^0_{CM} is the initial concentration of carcinogen molecules in the whole system, V_{CM} the volume of the dispersing carcinogen solution, N_A Avogadro's number, M_{CM} the molar weight of carcinogen molecules, and the subscript CM denotes carcinogen molecules; AO or BP. The solid lines for AO are the calculated ones using equation (21) with fitting parameters of $\tilde{n}_0$ and τ_0 determined by a least squares method. The cobalt chloride concentration (C_{Co}) dependences of $\tilde{n}_0$ and τ_0 for the adsorption of AO are shown in Figs. 20 and 21, respectively. At low C_{Co} (< 200 mM) $\tilde{n}_0$ is smaller than 1, whereas at high C_{Co} (>600 mM) $\tilde{n}_0$ is larger than 1, as shown in Fig. 4. τ_0 increases with increasing C_{Co} in the range less than 400mM, and is constant above that, as shown in Fig. 21. For the adsorption of BP, the observed adsorption behavior could not be expressed by equation (21), but well expressed by equation (27). Figure 6 (a) and (b) show the scaled plots of adsorption process for AO at the early stage at typical cobalt concentrations of 100 mM ($\tilde{n}_0 < 1$) and 1000 mM ($\tilde{n}_0 > 1$) for preparation. The straight lines in the plots of Figure 22 (a) are consistent with the theoretical equation (27). Figure 23 is the plot for AO adsorption suggested by theoretical equations (31) and (35) at the later stage. The straight lines also support the theory. The data for the adsorption of BP were not taken over the whole range including near equilibrium state.

3.5 Discussion

The rate of decrease of AO concentration C_{AO} in the dispersing solution decreases with increasing the concentration of cobalt chloride used for the gel preparation, as

shown in Fig. 18 (a). The entire processes of AO adsorptions are well expressed by the theoretically obtained scaled plot (21) with fitting parameters of $\tilde{n}_0$ and τ_0, as shown in Fig. 19 (a). Since AO molecules are cationic carcinogens, they are adsorbed by not only intercalation into the DNA double helices but also by electrostatic interaction between the negative charges of DNA and the positive charges of AO. Then, the AO molecule adsorption process well satisfies the assumptions (A) and (B). When the beads were prepared at high C_{Co}, the negative charges of DNA molecules should have been highly neutralized by cobalt cations before adsorption experiment: In the other words, the adsorption sites for electrostatic interaction is occupied by cobalt cations during the process of preparation of beads, resulting in larger $\tilde{n}_0$ at high C_{Co}. Note that $\tilde{n}_0$ is the ratio of the initial number of carcinogen molecules in the dispersing solutions to the number of the site of adsorption of carcinogen molecules in the beads. The sign of $\tilde{n}_0 - 1$ varies from negative to positive at around C_{Co} ~ 400 mM, as shown in Fig. 20. Thus, in the case of $\tilde{n}_0 < 1$, it is suggested that the carcinogen molecules in the dispersing solution are adsorbed completely to the beads in equilibrium, whereas in the case of $\tilde{n}_0 > 1$, a part of the adsorption sites of the beads are still vacant; the critical cobalt concentration for full occupancy in equilibrium is around 400 mM. Figure 21 shows that the time constant τ_0 increases with increasing cobalt concentration at low C_{Co} (< 400 mM) and is constant at high C_{Co} (> 400 mM). The increase of τ_0 with C_{Co} at low C_{Co} and saturation after full occupancy at high C_{Co} are attributed to the relation between the mobility k of AO in the DNA LCG and the DNA-LCG structure. Since in high C_{Co} LCG, the DNA and the cobalt concentrations are high, thermal diffusion motion of AO molecules are frequently blocked. Then, the mobility k decreases and

τ_0 increases with increasing C_{Co}. Figures 6 and 7 show asymptotic behaviors at early and later stages that are also consistent with the theoretical prediction. The root-square plots in Fig. 22 indicate that the adsorption process is limited by diffusion of carcinogen molecules in the beads. The straight lines in Fig. 23 for the later stage also supports the theoretical consideration; the adsorption process is represented by a power law function with the exponent 3/2 in the case of $\tilde{n}_0 > 1$ or by an exponential function in the case of $\tilde{n}_0 < 1$, though we cannot exclude other functions from the present limited time range of data for the later stage.

On the other hand, the adsorption process for BP was expressed by equation (27) for the initial stage. As clearly observed in Figs. 18 and 19, the time for reaching equilibrium is much larger for BP adsorption than AO adsorption. Paying attention to the solubility difference between AO and BP in water (solubility of BP is about 10^3 times smaller than AO), we obtain a simple explanation for the much difference of equilibrium times. In terms of the maximum solvable BP density ρ_{MAX} in the gel, the maximum of the osmotic pressure is given by $\pi_{MAX} = g(\rho_{MAX})$ (See equation (7)). When the osmotic pressure of BP in the dispersing medium is larger than π_{MAX}, the following extension for the osmotic pressure balance equation (11) is required;

$$k_B T \rho_s(t) = \sigma + \pi_{MAX} \tag{36}$$

where σ is the gel bead surface tension for the osmotic pressure of BP molecules. Then, we have

$$4\pi R^2 J(R) = \frac{4\pi kRr}{R-r}\pi_{MAX} = \frac{4\pi kR\left(1-n(t)/n_f\right)^{1/3}}{1-\left(1-n(t)/n_f\right)^{1/3}}\pi_{MAX} \tag{37}$$

and the scaled time development equation

$$\frac{d\tilde{n}}{d\tilde{t}} = \frac{\left(1-\tilde{n}\right)^{1/3}}{1-\left(1-\tilde{n}\right)^{1/3}} \tag{38}$$

where $\tilde{t} = t/\tau_1$ with

$$\tau_1 = \frac{1}{4\pi kRn_f \pi_{MAX}} \tag{39}$$

Note that n_0 does not appear in the above equations. From (38), we have

$$\tilde{t} = \frac{3}{2}\left[1-(1-\tilde{n}_0\tilde{v})^{2/3}\right]-\tilde{n}_0\tilde{v} \tag{40}$$

If the maximum osmotic pressure π_{MAX} is small, the "equilibrium time" τ_1 is large. Then, even for long time interval, we regard as $\tilde{t} \approx 0$, $\tilde{n} = \tilde{n}_0\tilde{v} \approx 0$. Therefore, we can adopt the approximation

$$\frac{3}{2}\left[1-(1-\tilde{n}_0\tilde{v})^{2/3}\right]-\tilde{n}_0\tilde{v} \approx \frac{1}{6}(\tilde{n}_0\tilde{v})^2 \tag{41}$$

and we have the following square behavior consisting with the result shown in Fig.3(b).

$$t \propto \tilde{v}^2 \qquad (t << \tau_1). \tag{42}$$

To evaluate the time constant τ_1, the BP adsorption behavior is analyzed on the basis of equation (40) and the two parameters $\tilde{n}_0$ and τ_1 are obtained by a least square method. We obtain the parameter values, $\tau_1 = 5.5\times10^6$s and $\tilde{n}_0 = 0.16$ for $C_{\mathrm{Co}} = 100$mM, and $\tau_1 = 4.0\times10^6$s and $\tilde{n}_0 = 0.20$ for $C_{\mathrm{Co}} = 1000$mM. Thus, expected large values of τ_1 are obtained. Using these parameters, the $\tilde{v}$ - $\tilde{t}$ relation for the BP adsorption is shown in Fig. 24. The theoretical curves given by (40) are also shown (the solid lines). Figure 24 indicates that the idea of the extended osmotic pressure balance (36) is valid. The time range of the observation is too narrow to obtain precise values of the parameters. To obtain the precise values, the data for large t region are required. In enough large t regions, the osmotic pressure of BP in the dispersing medium may be less than the maximum osmotic pressure π_{MAX} since ρ_s decreases. In these time regions, the theory for the AO adsorption expressed by

equation (21) comes to be suitable for explaining the BP adsorption behavior.

The consistence of experiments and theory also suggests that liquid crystallinity of DNA LCG does not affect the adsorption behavior seriously. The difference of the adsorption behavior between AO and BP is attributed to the solubility difference.

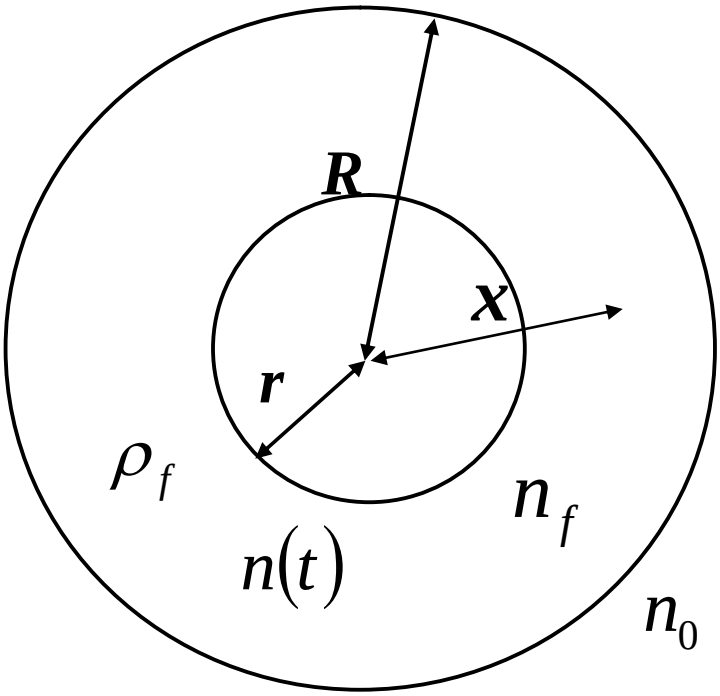

Figure 17 Schematic illustration of the adsorption system. n_0, n_f, r_f, and $n(t)$ denote the number of carcinogen molecules in the solution at the initial state, the maximum number of carcinogen molecules that the DNA LCG bead is capable to adsorb, the maximum number and the number of carcinogen molecules adsorbed to the bead at immersion time t, respectively.

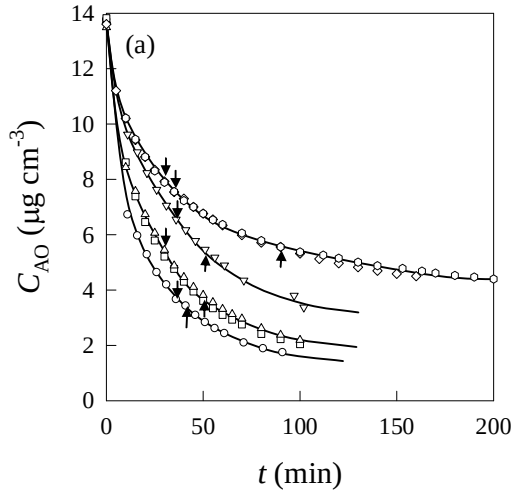

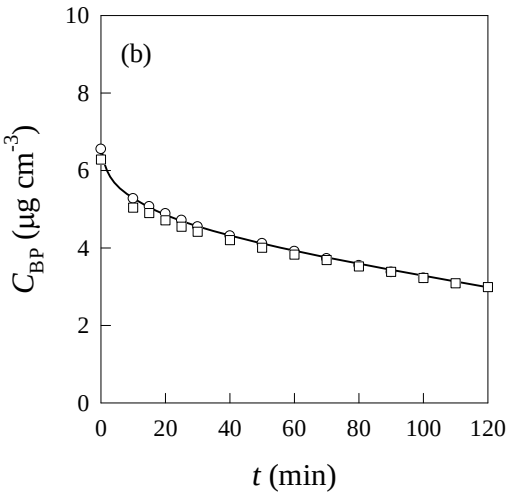

Figure 18 Time course of concentration of carcinogenic agents in medium: (a) AO for the DNA LCG beads prepared at C_{Co} = 50 mM (circle), 75 (square), 100 (triangle up), 200 (triangle down), 600 (diamond), and 1000 (hexagon); and (b) BP for the DNA LCG beads prepared at C_{Co} = 100mM (circles), and 1000 mM (squares), respectively. The solid curves are drawn to guide the eyes. The down-arrows indicate the terminal time of the early stage at which the time course is expressed by eq 27, and the up-arrows indicate the starting time of the later stage at which the time course is expressed by 31 or 35.

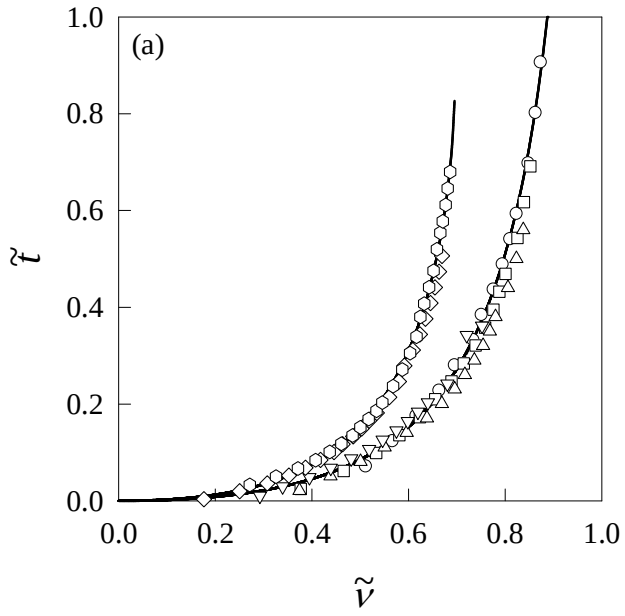

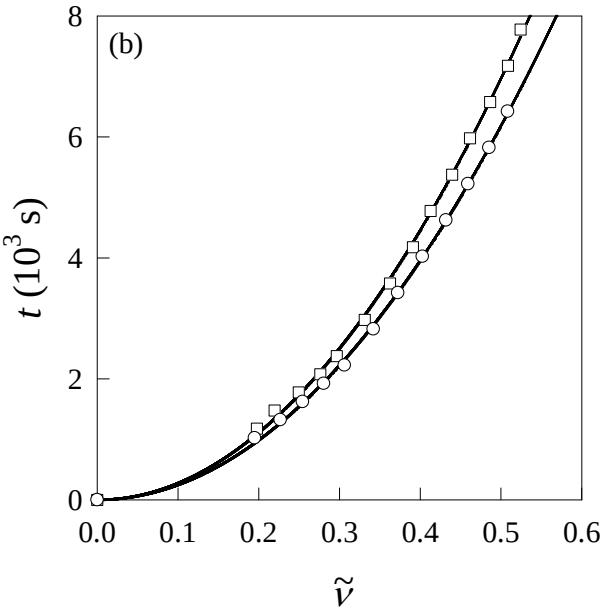

Figure 19 Time course of scaled number $\tilde{\nu} = \tilde{\nu}(\tilde{t})$ of adsorbed AO (a) and BP (b) to theDNA LCGbeads prepared at various cobalt chloride concentrations. The symbols denote the same meaning as the caption of Figure 2. The solid lines are calculated ones using eq 21 with fitting parameters for panel a, and eq 27 was used for panel b.

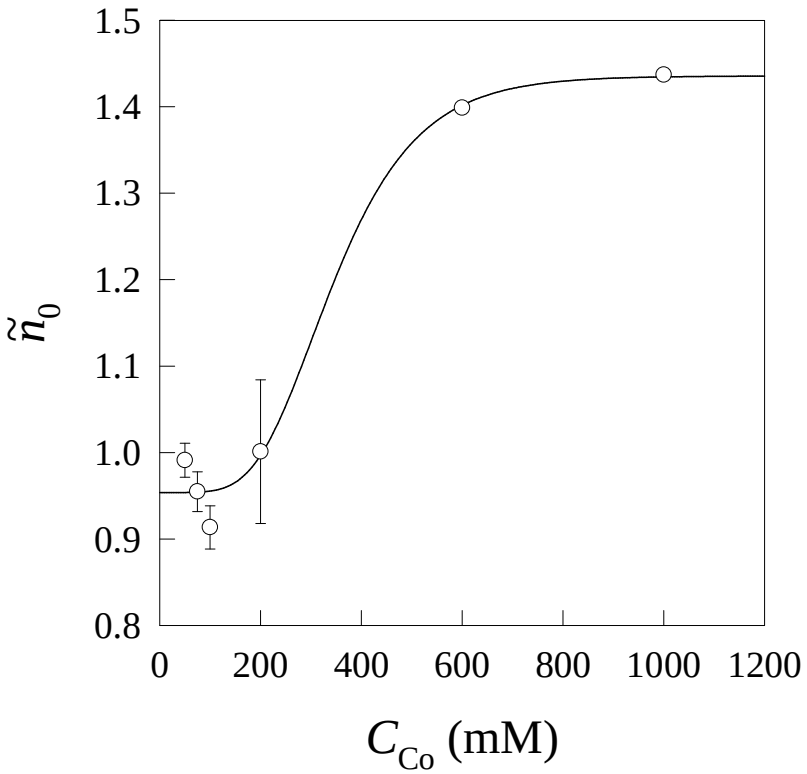

Figure 20 Scaled number of AO molecules $\tilde{n}_0$ determined by a least-squares method as a function of the cobalt chloride concentration used for gel preparation.

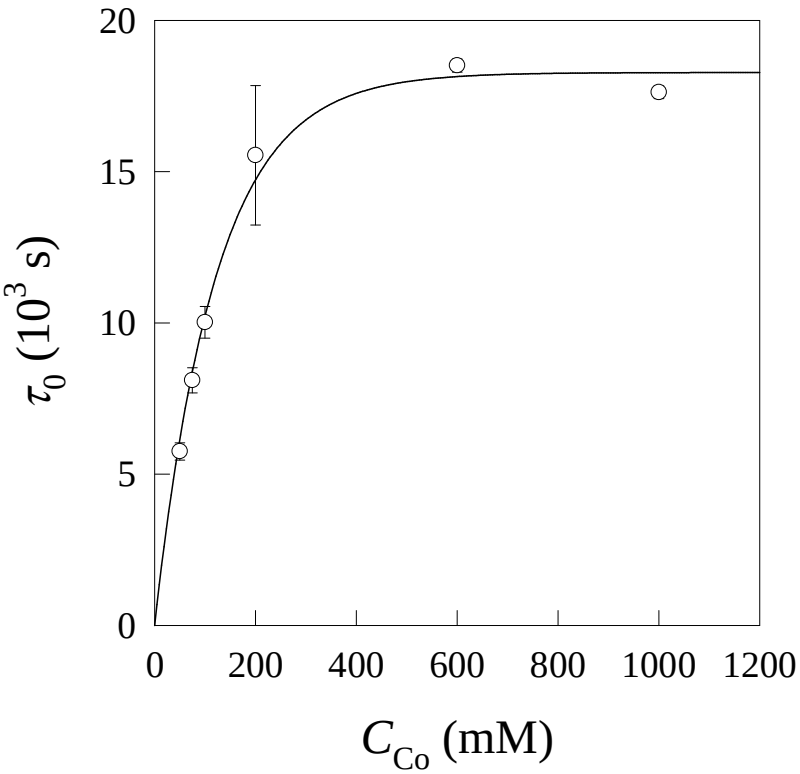

Figure 21 Time constant τ_0 in eq 21 for the adsorption of AO determined by a least-squares fit as a function of the cobalt chloride concentration used for gel preparation.

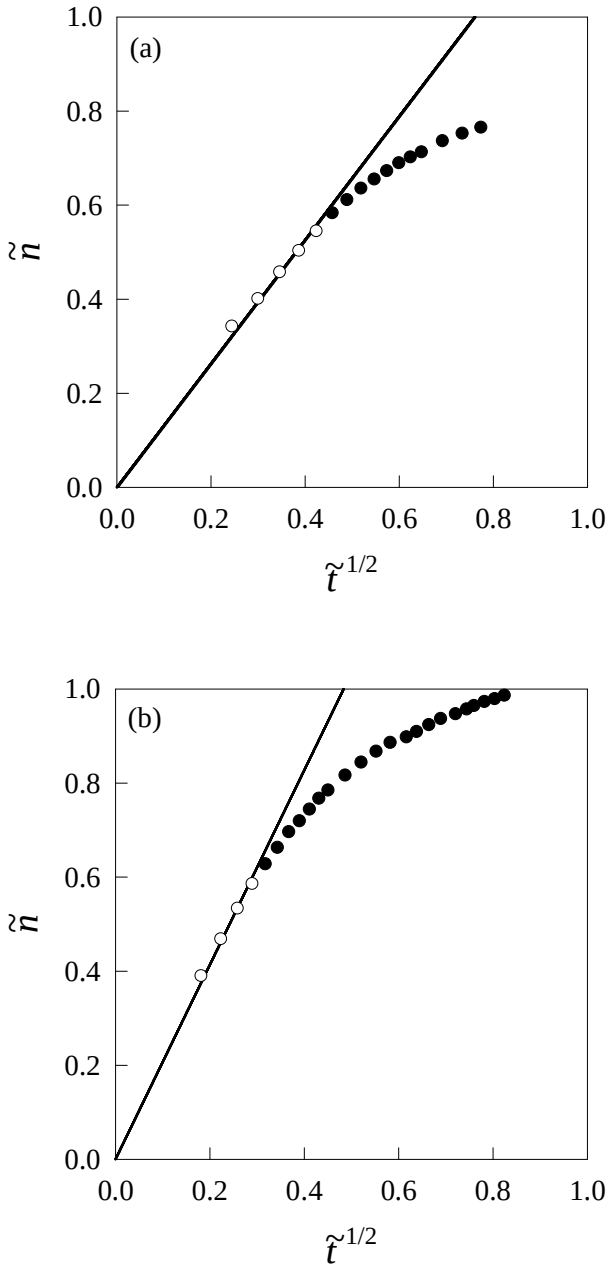

Figure 22 Scaled plots according to eq 27 for the early stage for adsorption of AO: (a) C_{Co} = 100 mM; (b) C_{Co} = 1000 mM.

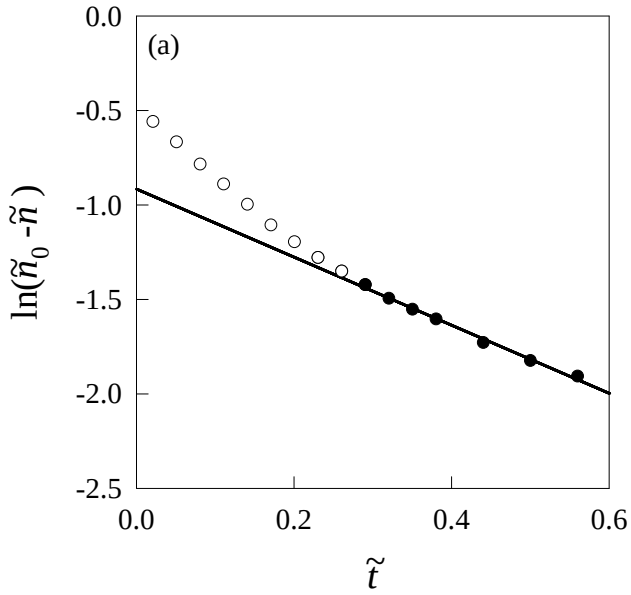

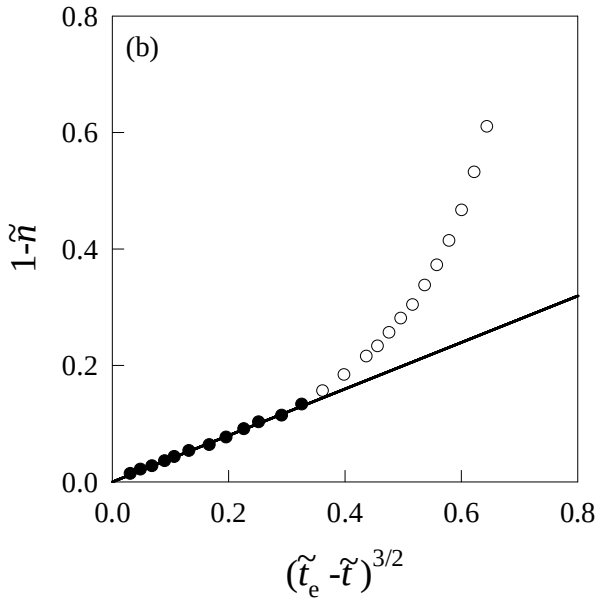

Figure 23 Scaled plots according to eqs 31 (a; C_{Co} = 100 mM) and 35 (b; C_{Co} = 1000 mM) for the final stage of the adsorption of AO.

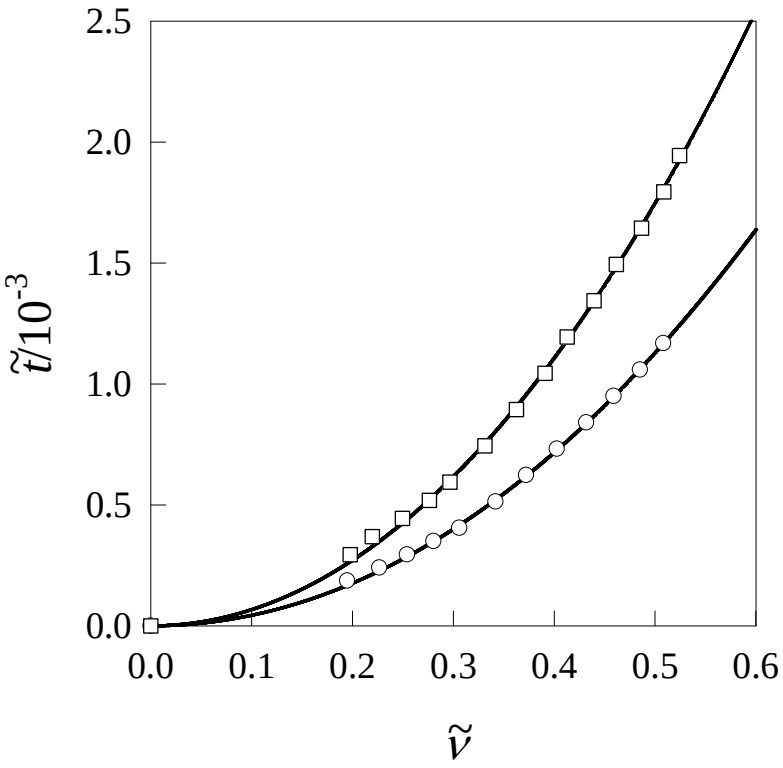

Figure 24 Time course of scaled number $\tilde{\nu} = \tilde{\nu}(\tilde{t})$ of adsorbed BP to the DNA LCG beads prepared at C_{Co} = 100 mM (circles) and 1000 mM (squares) cobalt chloride concentrations. The solid lines were calculated using eq 40 with fitting parameters.

Summary

In this thesis, liquid crystalline gelation of DNA has been studied both experimentally and theoretically. In Chapter 1, the optimum condition of liquid crystalline gelation of DNA aqueous solutions has been determined as a function of DNA weight fraction, concentration of cobalt chloride, and pH of DNA aqueous solutions, and the LCG property, such as swelling ratio, birefringence, thickness of LCG layer, Young's modulus and adsorption capacity of carcinogens also has been investigated. The liquid crystalline gelation of concentrated DNA aqueous solution was induced by dialysis into concentrated multivalent metal cations, such as Ca^{2+}, Mg^{2+}, Fe^{2+}, Co^{2+}, Ni^{2+}, Mn^{2+}, Zn^{2+}, Cu^{2+}, Dy^{2+}, and Al^{3+}, solutions. When the divalent transition metal cation, such as Co^{2+}, Ni^{2+}, and Zn^{2+}, were used as the solute of extradialytic solutions, the DNA liquid crystalline gel (LCG) consisted of an outer LCG layer and an inner amorphous gel (AG) layer. The swelling ratio of the DNA gel was rapidly decreased above pH 8.5, whereas the birefringence, the thickness, and Young's modulus of the LCG layer were drastically increased above pH 8.5. The results suggest that when divalent transition metal cations are used for preparation of DNA LCG, the DNA solutions must be in basic condition (pH>8.5).

In Chapter 2, the dynamics of dialysis-induced DNA liquid crystalline gelation was investigated both theoretically and experimentally. To analyze the dynamics experimentally, we used the DNA liquid crystalline gel (LCG) films prepared by immersing DNA aqueous borate solutions sandwiched between two parallel circular glass plates into cobalt chloride solutions and measured the time courses of the thickness, the weight fractions of DNA and cobalt cations, the birefringence and the turbidity of the film consisted of outer DNA LCG and inner DNA amorphous gel or

solution. To clarify the mechanism of the process forming LCG, the theory based on the non-equilibrium thermodynamics with “moving boundary picture” was modified, and the results were analyzed by the modified theory. It was found that the growth process of DNA LCG consists of two dynamics: The cobalt cation diffusion limited process at the early stage and the pH change limited process at the later stage.

In Chapter 3, the entire processes of adsorption of acridine orange (AO) to DNA LCG beads were well expressed by a theoretical scaled equation derived on the basis of non-equilibrium thermodynamics (the moving boundary picture). The dependence of cobalt chloride concentration used for preparation of the beads on the characteristic parameter $\tilde{n}_0$ of adsorption was attributed to adsorption site number difference in DNA LCG beads and τ_0 was attributed to the mobility difference of AO in DNA LCG beads. The adsorption behavior at the later stage depends on the ratio of the initial number of carcinogen molecules in the dispersing solution to the number of the site of adsorption of carcinogen molecules in the beads $\tilde{n}_0$. The adsorption behaviors of AO and of biphenyl (BP) are apparently different. However, the difference is simply due to the equilibrium time difference induced by the solubility difference of AO and BP in water. The two apparently-different adsorption behaviors were explained by the same theory based on the moving boundary picture. It is hoped to apply for its practical use.

In conclusion, the basic mechanism of DNA LCG formation and adsorption of carcinogens were clarified in this study.

References

(1) J. D. Watson, F. H. C. Crick, *Nature*, **1953**, *171*, 737.

(2) M. H. F. Wilkins, A. R. Stocker, H. R. Wilson, *Nature*, **1953**, *171*, 738.

(3) R. E. Franklin, R. Gosling, *Nature*, **1953**, *171*, 740.

(4) W. Saenger, *Principles of Nucleic Acid Structure*, Springer-Verlag, New York **1984**.

(5) O. Avery, C. MacLeod, M. McCarty, *J. Expt. Med*. **1944**, *79*, 137.

(6) M. Meselson, F. W. Stahl, *Proc. Natl. Acad. Sci. USA*, **1957**, *44*, 671.

(7) H. Kitamura, C. Iwamoto, N. Sakairi, S. Tokura, N. Nishi, *Int. J. Biol. Macromol*. **1996**, *18*,149.

(8) M. Yamada, K. Kato, M. Nomizu, K. Ohkawa, H. Yamamoto, N. Nishi, *Environ. Sci. Technol*. **2002**, *36*, 949.

(9) M. Yamada, K. Kato, K. Shindo, M. Nomizu, M. Haruki, N. Sakairi, K. Ohkawa, H. Yamamoto, N. Nishi, *Biomaterials*, **2001**, *22*, 3121.

(10) M. Yamada, K. Kato, M. Nomizu, K. Ohkawa, H. Yamamoto, N. Nishi, *Chem. Eur. J*., **2002**, *8*, 1407.

(11) D. Umeno, T. Kano, M. Maeda, *Anal. Chim. Acta*., **1998**, *365*, 101.

(12) Y. Okahata, T. Kobayashi, K. Tanaka, M. Shimomura, *J. Am. Chem. Soc*., **1998**, *20*, 241.

(13) P. Aich, S. L. Labiuk, L. W. Tari, L. J. T. Delbaere, W. J. Roesler, k. J. Falk, R. P. Steer, J. S. Lee, *J. Mol. Biol*, **1999**, *294*, 477.

(14) L. S. Lerman, *J. Mol. Biol*., **1961**, *3*, 18-30.

(15). H. W. Zimmerman, *Angew. Chem. Intl. Ed. Engl*., **1986**, *25*, 115.

(16) P. Brookers, P. D. Lawley, *Nature*, **1964**, *202*, 781.

(17) F. Livolant, A. Leforestier, Prog. Polym. Sci., **1996**, *21*, 1115.

(18) T. E. Strzelecka, M. W. Davidson, R. L. Rill, Nature, **1988**, *331*,457.

(19) R. L. Rill, *Proc. Natl. Acad. Sci. USA*, **1986**, *83*, 342.

(20) R. L. Rill, P. R. Hilliard, Jr., G. C. Levy, *J. Biol. Chem.*, **1983**, *258*, 250.

(21) S. S. Zakharova, W. Jesse, C. Backendorf, R. C. J. R. C. van der Maarel, *Biophys. J.* **2002**, *83*, 1119.

(22) T. Amiya, T. Tanaka, *Macromolecules*, **1987**, *20*,1162.

(23) M. G. Fried, V. A. Bloomfield, *Biopolymers*, **1984**, *23*, 2131.

(24) T. Dobashi, M. Nobe, H. Yoshihara, T. Yamamoto, A. Konno, *Langmuir*, **2004**, *20*, 6530.

(25) T. Dobashi, K. Furusawa, E. Kita, Y. Minamisawa, T. Yamamoto, *Langmuir*, **2007**, *23*, 1303.

(26) M. Nobe, T. Dobashi, T. Yamamoto, *Langmuir*, **2005**, *21*,8155.

(27) N. J. Turro, J. K. Barton, D. A. Tomalia, *Acc. Chem. Res.* **1991**, *24*, 332.

(28) C. Desfrancois, S. Carles, J. P. Schermann, *Chem. Rev.* **2000**, *100*, 3943.

(29) R. B. Macregor Jr., R. M. Clegg, T. M. Jovin, *Biochemistry*, **1987**, *26*, 4008.

(30) F. J. Meyer-Almes, D. Porschke, *Biochemistry*, **1993**, *32*, 4246.

(31) E. Braun, Y. Eichen, U. Sivan, G. Ben-Yosephy, *Nature*, **1998**, *391*,775.

(32) T. Dobashi, H. Yoshihara, M. Nobe, M. Koike, T. Yamamoto, *Langmuir*, **2005**, *21*, 2.

(33) M. Nobe, N. Kuroda, T. Dobashi, T. Yamamoto, A. Konno, M. Nakata, *Biomacromolecules*, **2005**, *6*, 3373.

(34) T. Kondo, In *Surface and Colloid Science*; E. Matijevic, Ed.; Plenum: New York, 1978; pp 1-43.

(35) V. A. Bloomfield, *Current Opinion in Structural Biology*, **1996**, *6*, 334.

(36) V. A. Bloomfield, *Biopolymers*, **1991**, *31*, 1471.

(37) V. A. Bloomfield, *Biopolymers*, **1997**, *44*, 269.

(38) J. G. Duguid, V. A. Bloomfield, J. M. Benevides, G. J. Thomas Jr., *Biophys. J.*, **1993**, *65*, 1916.

(39) J. G. Duguid, V. A. Bloomfield, J. M. Benevides, G. J. Thomas Jr., *Biophys. J.*, **1995**, *69*, 2623.

(40) M. Takahashi, K. Yoshikawa, V. V. Vasilevskaya, A. R. Khokhlov, *J. Phys. Chem.*, **1997**, *101*, 9396.

(41) G. R. Bartlett, *J. Biol. Chem.*, **1959**, *234*, 466.

(42) J. S. Lee, L. J. P. Latimer, R. S. Reid, *Biochem. Cell Biol.*, **1993**, *71*, 162.

(43) D. O. Wood, M. J. Dinsmore, G. A. Bare, J. S. Lee, *Nucleic Acid Res.* **2002**, *30*, 2244.

Acknowledgments

I would like to express my deepest sense of gratitude to Professor Toshiaki Dobashi for his continuous scientific instruction, encouragements, and precious discussion throughout all my research life in Dobashi Laboratory.

I would also like to express my thanks to Professor Takao Yamamoto for his fruitful theoretical discussion and education.

I wish to thank Dr Hiroyuki Takeno and Dr Yasuyuki Maki to their productive discussion.

I appreciate Dr Ken Terao at Osaka University for his experimental instruction and support.

I am grateful to Professor Shin Yagihara at Tokai University for his kindly help.

I am grateful to Professor emeritus Hiroshi Maeda at Kyusyu University for his valuable advice.

I am grateful to Dr Naotsugu Nagasawa at Japan Atomic Energy Agency for his experimental support.

I am thankful to my laboratory member and government officials at our department of Gunma University for their help.

This work was partly supported by Grant-in-Aid for Science Research from JSPS Research Fellowships for Young Scientists (# 058J6825)

Lastly I am grateful to my parent and my brother.

Publication List

関係論文

(1) T. Dobashi, **K. Furusawa**, E. Kita, Y. Minamisawa and T. Yamamoto; 『DNA liquid crystalline gel as adsorbent of carcinogenic agent』 *Langmuir*, **23**, 1303-1306, 2007.

(2) **K. Furusawa**, M. Wakamatsu, T. Dobashi, T. Yamamoto, 『Adsorption Kinetics of Carcinogens to DNA Liquid Crystalline Gel Beads』, *Langmuir*, **23**, 10081-10087, 2007.

(3) **K. Furusawa**, Y. Minamisawa, T. Dobashi, T. Yamamoto, 『Dynamics of DNA Liquid Crystalline Gelation』, *J. Phys. Chem.*, in press.

参考論文

(1) K. Terao, N. Nagasawa, H. Nishida, **K. Furusawa**, Y. Mori, Y. Fumio, T. Dobashi; 『Reagent free crosslinking of aqueous gelatin: manufacture and characteristics of gelatin gels irradiated with gamma ray and electron beam』 *J. Biomater Sci. Polym. Edition.*, **14**, 1197-1208, 2003.

(2) **K. Furusawa**, K. Terao, N. Nagasawa, F. Yoshii, K. Kubota, T. Dobashi; 『Nanometer-sized gelatin particles prepared by means of gamma-ray irradiation』 *Colloid and Polym. Sci.*, **283**, 229-233, 2004.

(3) **K. Furusawa**, T. Dobashi, S. Morishita, M. Oyama, T. Hashimoto, N. Shinyashiki, S. Yagihara, N. Nagasawa; 『Structural and kinetic modification of aqueous hydroxypropylmethylcellulose (HPMC) induced by electron beam irradiation』 *Physica* A, **353**, 9-20, 2005.

(4) **森下敏、海野裕哉、喜多理王、新屋敷直木、八木原晋、古澤和也、土橋敏明、長澤尚胤**; 『**誘電測定による電子線架橋** hydroxypropylmethylcellulose (HPMC)**ゲルの動的構造の研究**』 ***東海大学紀要***、**41**、106-112、2006.

(5) Y. Minamisawa, **K. Furusawa**, T. Yamamoto, T. Dobashi; 『Mono- and Multilayered Aluminum ion-induced liquid crystalline gel of DNA』 *Trans. MRS-J*, **31**, 739-741, 2006.

(6) Y. Umino, S. Morishita, R. Kita, N. Shinyashiki, S. Yagihara, **K. Furusawa**, T. Dobashi, N. Nagasawa; 『Water and chain dynamics in polymer network structure』 *Trans. MRS-J*, **31**, 767-770, 2006.

(7) Y. Maki, **K. Furusawa**, M. Wakamatsu, T. Yamamoto, T. Dobashi; 『Adsorption Kinetics of Carcinogenic Agents to DNA Gel Beads』 *Trans. MRS-J*, **32**, 799-802, 2007.

(8) **K. Furusawa**, Y. Maki, T. Yamamoto, T. Dobashi, 『**濃厚DNA水溶液の多価カチオン水溶液に対する透析に関するレオロジー的研究**』, Journal of Japanese Society of Biorheology, **21**, 4 **号掲載予定**

(9) **K. Furusawa**, E. Kita, T. Saheki, N. Nagasawa, N. Nishi, T. Dobashi, 『Carcinogen adsorbent prepared from DNA complex by gamma-ray irradiation』, *J. Biomater. Sci. Polym. Ed.*, **投稿中**